JOURNAL OF GEOPHYSICAL RESEARCH, VOL. 105, NO. D5, PAGES 6633–6653, MARCH 16, 2000

Impacts of biomass burning on tropospheric CO, NO_x, and O_3

Meredith Galanter

Atmospheric and Oceanic Sciences Program, Princeton University, Princeton, New Jersey

Hiram Levy II

Geophysical Fluid Dynamics Laboratory, Princeton, New Jersey

Gregory R. Carmichael

Center for Global and Regional Environmental Research, University of Iowa, Iowa City

Abstract. This study utilizes the National Oceanic and Atmospheric Administration Geophysical Fluid Dynamics Laboratory three-dimensional global chemical transport model to quantify the impacts of biomass burning on tropospheric concentrations of carbon monoxide (CO), nitrogen oxides (NO_x), and ozone (O_3). We construct updated global sources that emit 748 Tg CO/yr and 7.8 Tg N/yr in the surface layer. Both sources include six types of biomass: forest, savanna, fuelwood, agricultural residues, domestic crop residues (burned in the home for cooking and/or heating), and dried animal waste. Timing for the burning of forest, savanna, and agricultural residues is based upon regional cultural use of fire, vegetation type, local climate, and information gathered from satellite observations, while emissions from the burning of fuelwood, domestic crop residues, and dried animal waste are constant throughout the year. Based on agreement with observations, particularly of CO, we conclude that the collective uncertainty in our biomass burning sources is much less than the factor of two suggested by previous estimates of biomass burned in the tropics annually. Overall, biomass burning is a major source of CO and NO_x in the northern high latitudes during the summer and fall and in the tropics throughout most of the year. While it contributes more than 50% of both the NO_x and CO in the boundary layer over major source regions, it has a much larger global impact on the CO distribution in comparison to either NO_x or O_3, contributing 15 to 30% of the entire tropospheric CO background. The only significant biomass burning contribution to NO_x at 500 mbar, due to the short lifetime of NO_x in the lower troposphere, is a plume occurring July through October in the Southern Hemisphere subtropical free troposphere, stretching from South America to the western Pacific. The largest impacts on O_3 are limited to those regions where NO_x impacts are large as well. Near the surface, biomass burning indirectly contributes less than half of the total O_3 concentrations over major tropical source regions, up to 15% throughout the year in the tropics, and 10 to 20% throughout the Southern Hemisphere during September through November. At 500 mbar, the largest contribution to O_3 (20 - 30%) is correlated with the NO_x plume during July through November. Biomass burning contributes less than 15% of either NO_x or O_3 in the upper troposphere.

1. Introduction

Though lightning is known to be a natural contributor to biomass fires, today most fires are the result of deliberate human fire management practices, particularly in the tropical and subtropical regions. Public awareness of the environmental impacts of biomass burning and justified concern about its consequences are growing. Biomass burning serves a variety of purposes: clearing of forest and brushland for agricultural use, conversion of forests to agricultural and pastoral lands, energy production for cooking and heating, control of pests, insects, and weeds, nutrient mobilization, and the removal of brush and litter [*Crutzen and Andreae*, 1990].

Biomass burning on a wide scale causes significant regional pollution, often with deleterious impacts on the health and safety of the local population. Such effects include reduced visibility leading to transportation accidents [e.g., *Nichol*, 1998], as well as eye, skin, and respiratory ailments, which can result from smoke and particulates produced by the fires. On a global scale, biomass burning may have significant impacts on atmospheric chemistry and global climate. Loading of the atmosphere with nitrogen oxides (NO_x = NO+NO_2), carbon monoxide (CO), black and organic carbon, mineral ash, and volatile organic compounds, in addition to greenhouse gases such as nitrous oxide (N_2O), carbon dioxide (CO_2), and methane (CH_4), contributes to air pollution, global

Paper number 1999JD901113.
0148-0227/00/1999JD901113$09.00

warming, and acid rain [*World Meteorological Organization*, 1997; *Andreae*, 1991; *Crutzen and Andreae*, 1990; *Crutzen et al.*, 1985; *Greenberg et al.*, 1984; *Logan*, 1983; *Crutzen et al.*, 1979]. The oxidation of CH_4, CO, and other hydrocarbons in a NO_x-enriched environment leads to the production of tropospheric ozone, thus modifying the reactivity of the atmosphere. Rising levels of NO_x also lead to increased deposition of nitric acid, a major contributor to acid rain [e.g., *Galloway and Likens*, 1981]. Ozone (O_3), a secondary product of biomass burning, has been shown to decrease crop yields and cause respiratory problems [e.g., *McKee*, 1993; *Chameides et al.*, 1994]. With a growing population, the demand for land use is increasing, and the challenge of assessing the role of biomass burning in atmospheric chemistry, climate, and terrestrial ecology is becoming increasingly important.

It has been estimated that approximately 85% of biomass burning takes place in tropical countries [*Andreae*, 1991], and the tropics play a particularly important role in tropospheric chemistry [*Crutzen and Zimmerman*, 1991]. The importance of the tropics in atmospheric chemistry may be attributed to the high concentrations of water vapor, as well as the strong flux of incoming solar radiation, which produce high levels of OH in this region. Combined with this active photochemical environment, strong vertical mixing over source regions by convection and stronger winds aloft create the potential for tropical biomass burning to have large-scale impacts on air quality. In fact, biomass burning is believed to be the most important source of CO and NO_x in the tropics [*Crutzen and Carmichael*, 1993]. Although a number of measurement campaigns have been launched in recent years to investigate impacts and consequences of biomass burning (e.g., Transport and Atmospheric Chemistry Near the Equator - Atlantic (TRACE-A) and Southern African Fire-Atmosphere Research Initiative (SAFARI)), these programs are limited spatially and temporally and hampered by the difficulties in directly measuring such photochemically important species as OH and peroxyl radicals. Complementary use of field observations with atmospheric chemistry and transport model simulations permits quantification of biomass burning's impact on the atmosphere's physical and chemical state [*Crutzen and Carmichael*, 1993].

Several studies have produced global estimates of the biomass combustion taking place each year and the amount of trace gases consequently being released. *Logan* [1983] evaluated the contribution of several types of biomass burning to the global budget of nitrogen oxides in the troposphere. *Seiler and Crutzen* [1980] assessed the geographical distribution of biomass burning and attempted to quantify the amount of carbon produced and biomass burned from different sources using demographic and statistical data. *Crutzen and Andreae* [1990] estimated the emissions of CO_2, CO, hydrocarbons, and nitrogen compounds from biomass burning in the tropics. *Andreae* [1991] evaluated previous work done on this topic and estimated global amounts of several types of biomass burned annually, as well as estimating emissions from tropical and global biomass burning. *Hao and Liu* [1994] went a step further, not only quantifying the amount of deforestation, shifting cultivation, savanna fires, fuelwood combustion, and agricultural residue burning, but also providing a spatial and temporal database with a 5° x 5° resolution. This database, however, only covers the tropical regions of America, Africa, and Southeast Asia, while excluding China and Australia.

As part of the current study, two biomass burning sources were generated for use with the Geophysical Fluid Dynamics Laboratory global chemical transport model (GFDL GCTM) and are described in detail in section 3 of this paper. Our sources cover the globe and include six types of biomass: forest, savanna, fuelwood, agricultural residues, domestic crop residues (burned in the home for cooking or heating), and animal waste. In addition, we specify the regional temporal variability of the sources based largely on the work of *Richardson* [1994]. The GFDL GCTM was then used to simulate the direct impact of biomass burning on global CO and NO_x distributions, as well as its indirect influence on the global O_3 distribution as described in sections 4, 5, and 6, respectively. Section 7 comments on the uncertainty of the biomass burning sources, and section 8 presents a summary of our conclusions.

2. Global Chemical Transport Model

The National Oceanic and Atmospheric Administration (NOAA) Geophysical Fluid Dynamics Laboratory global chemical transport model (GFDL GCTM) is used, in separate integrations, to simulate global fields of carbon monoxide (CO), nitrogen oxides (NO_x), and ozone (O_3). Nonmethane hydrocarbons (NMHC) are not explicitly included in the OH chemistries of any of the simulations, though acetone is included in O_3 production and NMHC are included in peroxyacetyl nitrate (PAN) formation. The GCTM has a horizontal resolution of ~ 265 km x 265 km and 11 sigma (terrain following) levels in the vertical at standard pressures (thicknesses range) of 990 mbar (1000-981), 940 mbar (981-902), 835 mbar (902-773), 685 mbar (773-607), 500 mbar (607-412), 315 mbar (412-241), 190 mbar (241-150), 110 mbar (150-81), 65 mbar (81-52), 38 mbar (52-27), and 10 mbar (27-0) [see *Mahlman and Moxim*, 1978; *Levy et al.*, 1982, 1985; *Levy and Moxim*, 1989]. The model is driven by 12 months of 6-hour time-averaged wind, temperature, and precipitation fields from a general circulation model (see *Manabe et al.* [1974] and *Manabe and Holloway* [1975] for details of the parent general circulation model (GCM)).

The transport module is second order in the horizontal and fourth order in the vertical for resolved (grid scale) advection [see *Mahlman and Moxim*, 1978, section 3], and although neither the parent GCM nor the GCTM contain diurnal insolation or interannual variability, the self-consistent three-dimensional wind, temperature, and precipitation fields capture large-scale transport due to extratropical cyclones and synoptic meteorology in general [*Moxim*, 1990; *Moxim et al.*, 1996]. While the relatively high resolution of the GCTM is able to simulate large-scale synoptic features of weather, it is not able to resolve finer details such as squall lines or moist convection and turbulence on their normally observed scales, a difficulty that is characteristic of all global models. These subgrid-scale processes are represented by parameterizations based on resolved grid-scale variables and are considered approximate representations of the actual physical processes. The model includes diffusion-based parameterizations for horizontal subgrid-scale transport and vertical subgrid-scale transport due to moist and dry convection throughout the troposphere, and shear-dependent mixing in the boundary layer [see *Levy et al.*, 1985; *Kasibhatla et al.*, 1996, and references therein]. The subgrid-scale transport due to moist and dry convection, an

important process in the tropical biomass burning regions, has been shown to realistically capture the vertical distribution of radon over the summer continent and the upper tropospheric distribution of CO mixing ratios over South America during the burning season (see the Appendix in *Levy et al.* [1999] for details).

The GCTM simulation of CO includes sources from biomass burning (748 Tg CO/yr), fossil fuel (300 Tg CO/yr), biogenic hydrocarbon oxidation (683 Tg/yr), and CH_4 oxidation (758 Tg/yr) with OH oxidation of CO providing the only sink (see T.A. Holloway et al., Global distribution of carbon monoxide, submitted to *Journal of Geophysical Research*, 1999) (hereinafter referred to as Holloway et al. (submitted manuscript, 1999)). The OH distribution is based on three-dimensional monthly varying fields given by *Spivakovsky et al.* [1990] with a uniform increase of 15% to agree with a methyl chloroform lifetime of 4.8 years [*Prinn et al.*, 1995]. We take 1990 as our base year for emission estimates for both the CO and NO_x (described below) simulations. Results from simulations using these emission sources compare favorably with ground-based measurements from the NOAA Climate Monitoring and Diagnostics Laboratory (CMDL) global cooperative flask sampling network and from the Jungfraujoch observatory station of the Swiss Federal Laboratories for Materials Testing and Research (EMPA) (93% of seasonally averaged datapoints within ±25%), and with aircraft data from the NASA Global Tropospheric Experiment (GTE) (79% of regionally averaged datapoints within ±25%) [*Novelli et al.*, 1992; Holloway et al., submitted manuscript, 1999].

The GCTM simulation of NO_x has already been described in detail [*Levy et al.*, 1999]. The GCTM transports three families of tracers, NO_x, PAN, and nitric acid (HNO_3); represents the chemical interconversions among these families by effective first-order rate coefficients that have been precalculated off-line; removes HNO_3 by wet deposition and all three by dry deposition; and includes sources from fossil fuel (22.4 Tg N/yr), biomass burning (7.8 Tg N/yr), soil-biogenic emission (5 Tg N/yr), lightning (4 Tg N/yr), aircraft emissions (0.45 Tg N/yr), and stratospheric injection (0.65 Tg N/yr). The simulated NO_x fields are in reasonable agreement with observations (~ 50% of the comparisons within 25% error limits, and ~ 75% within 50% error limits), show no systematic global biases, and exhibit the observed vertical profiles in the troposphere. The precalculated monthly mean OH fields used in the NO_x simulation have a methyl chloroform lifetime of 6.3 years. The 30% increase in OH needed to reduce the methyl chloroform lifetime to 4.8 years would reduce the impact of biomass burning on NO_x in the mid and upper troposphere by at most 10 - 17%. This is discussed in more detail in section 5 of *Levy et al.* [1999].

The GCTM simulation of tropospheric O_3 chemistry has also already been described elsewhere [*Yienger et al.*, 1999; *Levy et al.*, 1997; *Klonecki and Levy*, 1997; *Kasibhatla et al.*, 1996], and we summarize the four components here. Irreversible stratospheric injection of O_3 (629 Tg O_3/yr) occurs primarily at mid and high latitudes during winter and spring. The CH_4-CO/acetone-H_2O-NO_x-based 24-hour averaged rates of ozone production and destruction in the background troposphere (NO_x < 200 parts per trillion by volume (pptv); isoprene < 100 pptv) are interpolated each time step from precalculated tables [*Klonecki and Levy*, 1997] using the model's instantaneous O_3 levels, 6-hour averaged NO_x and CO concentrations from separate simulations (as described above), and monthly averaged H_2O concentrations from observations [*Oort*, 1983; *Soden and Bretherton*, 1996]. These O_3 chemical rates respond to all GCTM generated fluctuations in O_3, NO_x, and CO. While observed monthly mean H_2O does not include all of these fluctuations, the dominant variations with height, latitude, and season are captured. The parameterized net production of O_3 in the polluted boundary layer depends on the rate of NO_2 oxidation to HNO_3 by OH and provides realistic levels of O_3, which are then available for regional and global transport. Surface dry deposition, which depends on month and vegetation [*Matthews*, 1983], is calculated using a drag coefficient formulation for surface exchange [*Levy and Moxim*, 1989], and a standard resistance in series model for deposition velocities [*Wesely and Hicks*, 1977; *Wesely*, 1989]. Comparisons with over 300 seasonal observations from over 30 ozonesonde sites, 12 surface sites, and the TRACE-A aircraft mission find almost 90% of the model's simulated values agreeing within ± 25% with the observations [*Yienger et al.*, 1999; H. Levy et al., manuscript in preparation, 1999].

3. Biomass Burning Sources

The original 1° x 1° CO biomass burning source of 647 Tg CO/yr (J.A. Logan, personal communication, 1990) was a preliminary compilation which was then converted to a NO_x source [*Levy et al.*, 1991, and references therein]. Both biomass burning sources emitted a total biomass burning surface flux in each grid box (see *Dignon and Penner* [1991, and references therein] for a detailed description of the source construction). These original sources have been modified extensively as described in this section.

To account for the different types of biomass included in the source, the biomass burning sources were partitioned into forest, savanna, fuelwood, and agricultural residues for the tropics, based on the percentage of each type per model grid box from the 5° x 5° database of *Hao and Liu* [1994]. In Asia, estimates for CO and NO_x from biofuels were added to each source [*Streets and Waldhoff*, 1998]. The biofuels include three different types: fuelwood, crop residues, and dried animal waste (dung). *Streets and Waldhoff* [1998] report a detailed regional inventory for 1990 based on the burning of these biofuels in the home for cooking and/or heating. Their fuelwood estimates replaced the previous source in Asia, increasing the emissions from the burning of fuelwood in Asia from 33 to 59 Tg of CO/yr for the CO biomass burning source, while their estimates for Asian emissions from domestic crop residues and animal waste were added to the original sources based on location. Based on a nationwide and all-year-round domestic biofuel consumptions study in 1996 and 1997, *Marufu et al.* [1999] report that the burning of biofuels, predominately fuelwood, is the major source of CO and CO_2 emissions in Zimbabwe with emissions of 0.4 Tg CO-C/yr and 5.3 Gg NO-N/yr. While our biomass burning source does not include the burning of domestic residues or dried animal waste in that region, it does include fuelwood in Zimbabwe and the rest of the tropics. Although biofuels combustion may be the dominant source of CO emissions in Zimbabwe, they only make up to 1% of the CO emissions for the southern African region and the burning of domestic residues and dried animal waste is even a much smaller fraction. In the extratrop-

Table 1. Breakdown of CO Model Biomass Burning Source Showing Contribution of Each Type of Biomass.

Biomass Source Type	Original Biomass Source, Tg of CO	1999 Biomass Source, Tg of CO (% of Total)
Forest		296 (~40)
Savanna		258 (~34)
Fuelwood		88 (~12)
Agricultural residues		31 (~4)
Domestic crop residues		62 (~8)
Animal waste		12 (~2)
Total	647	748

ics the original biomass burning sources contained forest and fuelwood and were not modified. However, for budget calculations the biomass is considered to be forest only. High-altitude emissions from the Andes Mountains (>2.5 km model altitude) were removed from both sources because the release of biomass burning emissions into the free troposphere has not been observed in this region. Overall, the changes made to the CO biomass burning source increased the CO emissions by 101 Tg of CO/yr (see Table 1), from the original source of 647 Tg CO/yr (J.A. Logan, personal communication, 1990).

We specified the temporal distribution of burning by dividing the globe into 20 regions based on broad similarities in vegetation type, cultural patterns, and climate (see Figure 1). Based on these considerations, each region was then assigned a burning season with a fraction each month of the total annual forest, savanna, and agricultural residues, with a maximum usually occurring during the middle of the season (see Table 2). Timing estimates for the burning of forest, savanna, and agricultural residues are based largely on the work of *Richardson* [1994, and references therein]. The timing of the burning seasons is based on regional cultural use of fire, vegetation type, local climate, and information gathered from satellite observations [e.g., *Malingreau et al.*, 1989; *Richardson*, 1994]. The timing for Central America (region 7 in Figure 1) and Southeast Asia were modified from Richardson's timing based on the work of *Hao and Liu* [1994]. The monthly fractional distribution of biomass burning was altered for the region containing Southeast Africa and Madagascar and the region of southwest Africa, based on satellite observations (J.R. Olson, personal communication, 1998). The Northern Hemisphere (NH) and Southern Hemisphere (SH) extratropical regions' burning are distributed through a 4-month burning season during the respective hemisphere's summer months. The Indonesian and Australian burning seasons are based on satellite observations as well as field measurements of emissions from biomass burning [*Olson et al.*, 1999; *Taylor and Zimmerman*, 1991; *Melinotte et al.*, 1997]. Emissions from fuelwood, domestic crop residues, and animal waste are distributed evenly over the 12 months of the year in all regions.

Estimating timing of the source involves some uncertainty due to lack of accurate information concerning the regularity of burning in certain regions. In comparing our new source to the 5° x 5° database of *Hao and Liu* [1994] for the tropics, we find that the burning seasons in most regions overlap, although the majority of the burning seasons in our source are shorter than the 6-month burning periods assigned by Hao and Liu. *Hao and Liu* [1994] prescribe 6-month burning periods for their database based on rainfall data and distribute a percentage of biomass burned in each month corresponding to the distribution of surface ozone concentrations observed at three African sites and two South American sites. In most of Africa, burning in our source usually peaks 1 month prior to the peak in the Hao and Liu source. *Hsu et al.* [1999] report that smoke generated from savanna burning in southern Africa peaks between June and October based on comparisons of data from the Total Ozone Mapping Spectrometer (TOMS) aerosol index and Sun-photometer aerosol optical thickness for 1996 and 1997, which overlaps with the seasonality we prescribe for regions 10, 11, and 12 in Figure 1 and Table 2. Additionally, *Herman et al.* [1997] determined the burning season for southern Africa (0°-35°S, 10°E-40°E) as June through September based on analysis of 340- and 380-nm radiances from the TOMS data for the years 1979-1993.

In the northern Sudan/Sahel region of Africa (region 5 in Figure 1), the *Hao and Liu* [1994] source predicts peak burn-

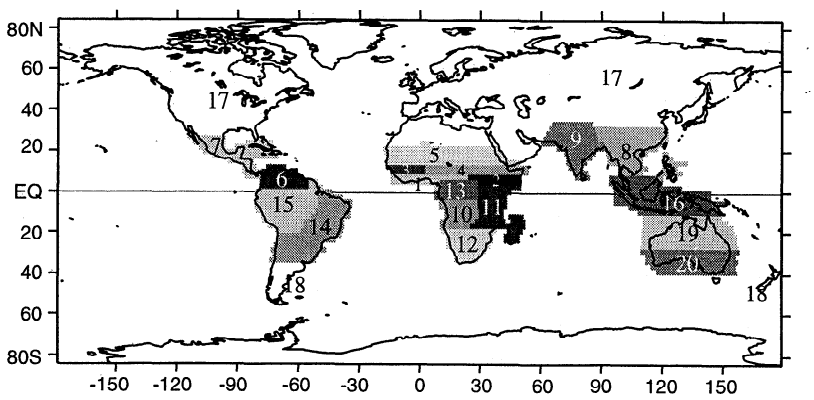

Figure 1. Biomass burning regions in the GCTM biomass burning source. The region numbers also refer to Table 2. Regions were designated by broad similarities in vegetation type, cultural patterns, and climate.

Table 2. Biomass Burning Calendar Depicting the Timing Distribution of the Model's Biomass Source.

Region	Jan.	Feb.	March	April	May	June	July	Aug.	Sept.	Oct.	Nov.	Dec.	Tg CO/yr	Tg NO_x/yr
1. Guinea savanna, west Africa	0.5	0.5											20.8	0.19
2. Guinea savanna, east North Africa	0.25	0.5	0.25										14.9	0.13
3. Southern Sudan, west Africa	0.375	0.375	0.125									0.125	14.6	0.13
4. Southern Sudan, east North Africa	0.25	0.25	0.25	0.125								0.125	49.6	0.45
5. Northern Sudan, Sahel	0.25									0.25	0.25	0.25	39.6	0.35
6. Northern South America		0.1	0.3	0.3									20.2	0.26
7. Central America			0.5	0.5									18.5	0.24
8. SE Asia	0.1	0.25	0.3	0.25	0.1								92.9	0.75
9. India	0.125	0.25	0.25	0.25	0.125								72.2	0.47
10. SW Africa						0.15	0.15	0.4	0.3				25.5	0.33
11. SE Africa/ Madagascar								0.3	0.4	0.15	0.15		51.6	0.66
12. South Africa						0.1	0.2	0.2	0.2	0.2	0.1		36.5	0.47
13. Equatorial Africa	0.25					0.25	0.25					0.25	15.2	0.17
14. Brazilian Cerrado						0.05	0.05	0.3	0.3	0.3			65.1	0.83
15. Amazon Basin							0.2	0.4	0.4				29.1	0.27
16. Indonesia							0.15	0.35	0.35	0.15			24.8	0.25
17. NH extratropics						0.2	0.3	0.3	0.2				120.6	1.26
18. SH extratropics	0.3	0.3	0.2									0.2	7.1	0.01
19. Northern Australia							0.15	0.2	0.3	0.2	0.15		27.1	0.35
20. Southern Australia	0.2	0.2	0.3	0.15								0.15	0.6	0.00

The last two columns indicate the amount of biomass burned in each respective region in units of Tg CO/yr and Tg NO_x/yr, respectively. The numbers represent the fraction of the annual forest, savanna, and agricultural residues burned during the particular month of the burning season. Fuelwood, domestic crop residues, and animal waste burning are distributed evenly over the 12 months of the year.

ing from March to May for areas north of 5°N in Africa, whereas burning in our source occurs from October through January (see Table 2). Our prescribed burning in this northern Sudan/Sahel region does agree, however, with the average biomass burning seasonality determined by *Cooke et al.* [1996] from remote sensing data of active vegetation fires on the African continent between November 1984 and October 1989. In addition, *Herman et al.* [1997] report that burning peaks for this region (0°-10°N, 15°W-20°E) in January to February based on TOMS data. This region is arid with a low

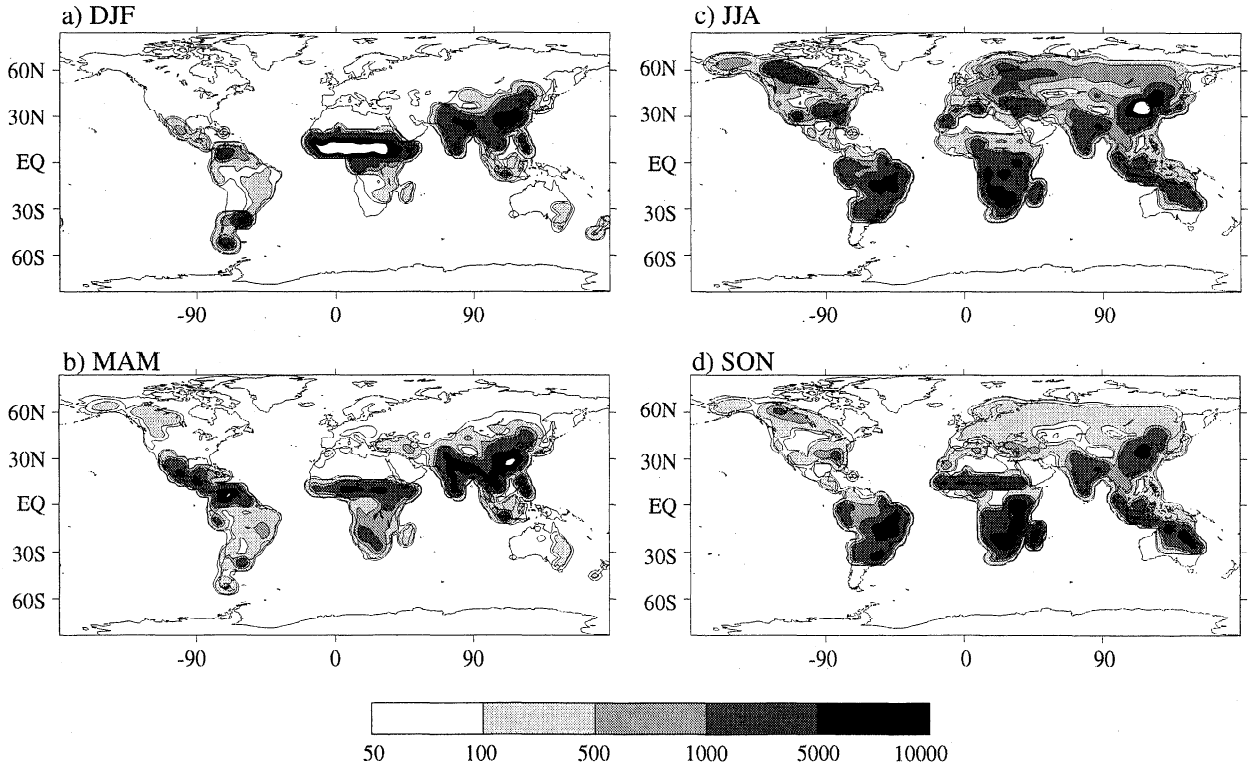

Figure 2. CO biomass burning source input to GCTM summed over each season in kg/km^2 (white within black denotes values greater than 10,000 kg/km^2/season) for (a) December, January, and February, (b) March, April, and May, (c) June, July, and August, and (d) September, October, and November.

production of annual grasses, widely used for raising cattle [*Menaut et al.*, 1991], and a long dry season beginning as early as October or November [*Richardson*, 1994]. The migration of herds results in a general trampling of vegetation a few months into the dry season [*Menaut et al.*, 1991], thus the burning season is prescribed to end in January.

The timing of our source is also in direct disagreement with the *Hao and Liu* [1994] database in equatorial Africa (region 13 in Figure 1 and Table 2). Hao and Liu's source has March as the peak month of burning 0°-5°N in Africa, and September for 0°-5°S. Precipitation data over this equatorial region records largely biennial behavior, with prescribed burning in our source occurring in the dry seasons in June through July and December through January [*Richardson*, 1994]. This timing is in agreement with the biomass burning seasonality reported by *Cooke et al.* [1996] for this region. *Herman et al.*'s [1997] analyses of TOMS data from 1979 to 1993 show peaks in biomass burning during December, January, and February for western equatorial Africa though the signal is complicated by desert dust. Their data also show an increase in UV-absorbing aerosols near the equator in June, July, and August.

Other tropical regions' burning seasons in the *Hao and Liu* [1994] source are in reasonable agreement with our timing. Additionally, *Herman et al.* [1997] analyses show agreement or overlap with our prescribed timing for Southeast Asia and South America.

Figures 2a - 2d show a seasonal breakdown of the model's CO biomass burning source (748 Tg CO/yr) in units of kg/km^2 season (where we define a season as 3 months: DJF, December, January, February; MAM, March, April, May; JJA, June, July, August; SON, September, October, November). Overall, the largest concentrations of emissions are found in the tropical regions of South America, Africa, Asia, and Australia. During DJF (Figure 2a) the most significant burning is taking place across parts of northern Africa. *Menaut et al.* [1991] describe most of this area as a zone of high grass production and severe annual burnings. Regions where grass production is low are mostly covered in shrubs, drought-deciduous woodland, and/or open grasslands [*Matthews*, 1985]. High concentrations of biomass burning are also seen in continental Southeast Asia, including India. The smaller signals seen over Indonesia, Central America, and South America arise from the burning of biofuels. In MAM (Figure 2b), Central America, northern South America, India and Southeast Asia experience the height of their burning seasons. In Southeast Asia the vegetation is predominantly tropical and subtropical evergreen and needle-leaved forests, while most of India is covered by tropical and subtropical drought-deciduous forest [*Matthews*, 1985]. Large concentrations of biofuels occurring in Asia make it a particularly rich source of CO from biomass burning [*Streets and Waldhoff*, 1998]. In South America, rainforest, drought-deciduous forest, and woody-tree-covered grasslands comprise most of the biomass in the region [*Matthews*, 1985; *Soares*, 1990], while Central America is predominately tropical forest. In JJA the NH extratropics, Amazon Basin, southern Africa, Indonesia, and Australia all exhibit high concentrations of biomass burning (see Figure 2c). Forest fires are the predominant source of biomass burning in the NH extratropics. Burning occurring in Australia is primarily of savanna grasslands. Finally, in SON, large concentrations of biomass burning are seen in the Brazilian Cerrado, Amazon Basin, southeast Africa, Indonesia, and Australia (Figure 2d). Large-scale fires in the savannas of Africa are dependent on drought

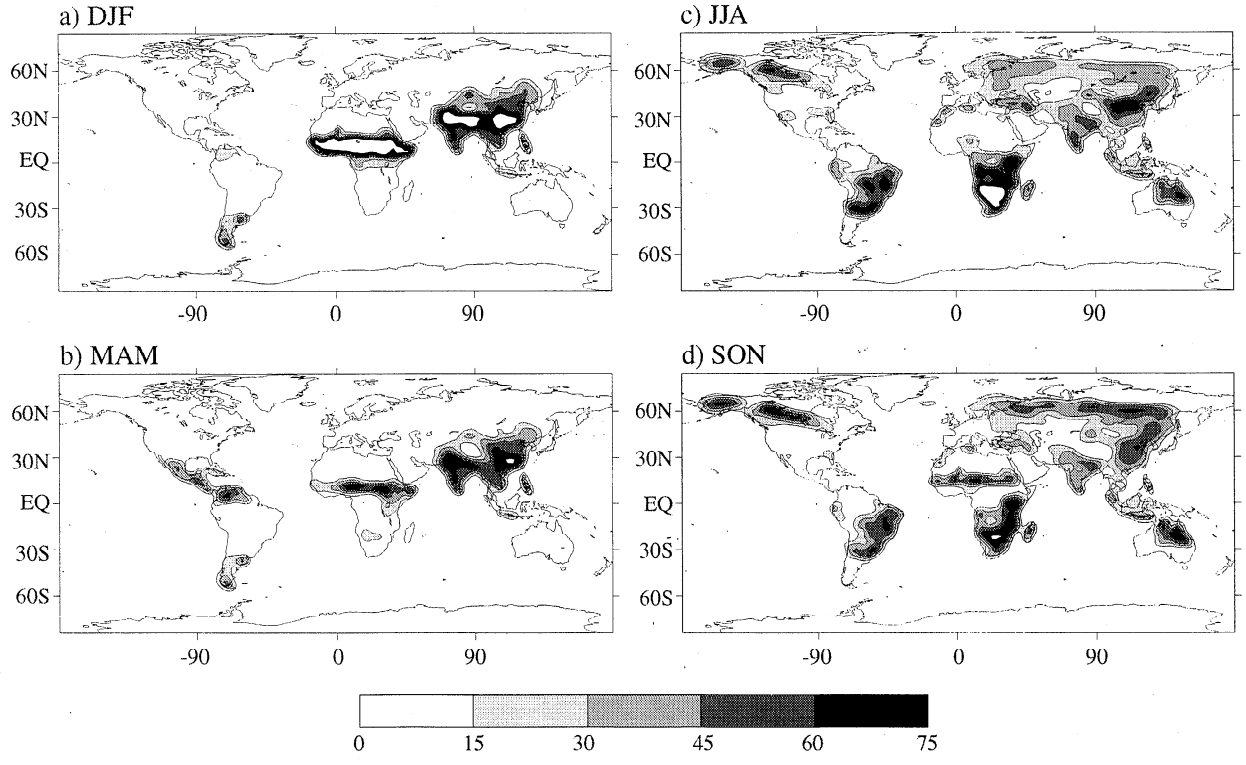

Figure 3. Percent contribution of biomass burning to all CO sources (white within black denotes values greater than 75%) for (a) December, January, and February, (b) March, April, and May, (c) June, July, and August, and (d) September, October, and November.

Table 3. Breakdown of NO_x Model Biomass Burning Source Showing the Contribution from Each Type of Biomass.

Biomass Source Type	Original Biomass Source Tg of N	1998 Biomass Source Tg of N (% of total)
Forest		3.62 (~47)
Savanna		2.97 (~38)
Fuelwood		0.49 (~6)
Agricultural residues		0.39 (~5)
Domestic crop residues		0.23 (~3)
Animal waste		0.05 (~0.7)
Total	8.5	7.8

conditions and occur frequently, though they are controlled in areas of large populations.

The seasonal percent contribution of biomass burning to the total CO sources in the model is shown in Figures 3a - 3d. Although the biomass burning source makes up approximately 31% of the total CO emissions (from all sources) annually, this source is concentrated in the tropics and can seasonally contribute over 75% in some tropical regions. As follows from the high concentrations seen in Figure 2, parts of Africa and Asia are affected by CO from biomass burning more than any other source in DJF, MAM, and SON. The biomass burning source shows the largest contribution to the total CO sources in Africa, with up to 80% in DJF (Figure 3a), as well as in JJA (Figure 3c). The large concentrations of biofuels in Asia again contribute to a large release of CO in the region. In JJA the SH sees significant contributions of biomass burning in southern Africa (> 75%), Australia (> 30%), and South America (> 30%). The largest percentage contribution of biomass burning to CO emissions in the NH extratropics occurs in SON (Figure 3d).

In addition to CO, nitrogen oxides (NO_x) are an important by-product of biomass burning. We estimate that the biomass burning source has increased from a preindustrial level of ~ 1 Tg N/yr [*Galloway et al.*, 1995] to a current level of 7.8 Tg N/yr. The same 1° x 1° CO biomass burning source (J.A. Logan, personal communication, 1990) used as a starting point for our revised CO biomass burning source, also served as the basis for our NO_x source. To convert the original CO source into the preliminary NO_x source, we used emission ratios of NO_x/CO_2 (0.002 [*Hao et al.*, 1990]) and CO/CO_2 (0.078 [*Andreae et al.*, 1988]). This early NO_x source of 8.5 Tg N/yr [*Levy et al.*, 1991] has been reduced by 0.7 Tg N/yr because of a decrease in emissions from the savannas of northern Africa, based on recent measurements of NO_x/CO_2 ratios in the Ivory Coast [*Delmas et al.*, 1995]. The present study updates these early NO_x emissions estimates as mentioned above. The NO_x biomass burning source was apportioned based on *Hao and Liu* [1994] percentages of fuelwood, forest, savanna, and agricultural residues in the tropics, and *Streets and Waldhoff* [1998] estimates for NO_x emissions from biofuels in Asia were added. Again, the highest concentrations in the source occur in the tropics. Table 3 shows a breakdown of the biomass types in the model and their magnitude. The seasonal distribution of the model's NO_x biomass burning source is the

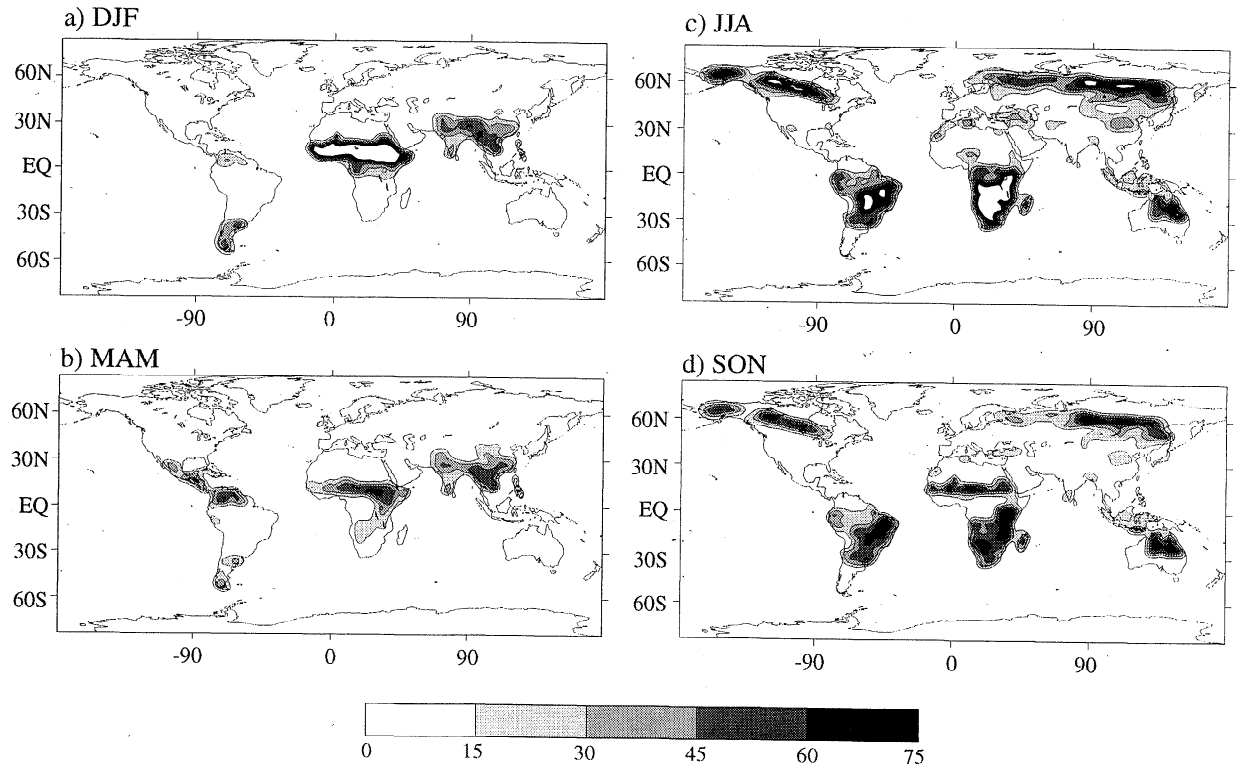

Figure 4. Percent contribution of biomass burning to all NO_x sources (white within black denotes values greater than 75%) for (a) December, January, and February, (b) March, April, and May, (c) June, July, and August, and (d) September, October, and November.

same as in Figures 2a - 2d shown above, with the exception of the decreased burning in northern Africa.

Overall, the NO_x biomass burning source contributes approximately 19% to the total of the NO_x sources in the model. However, NO_x emissions from biomass burning can be much more dominant, and thus have more impact, in regions where burning is prevalent. Figures 4a - 4d show the seasonal percent contribution of the biomass burning source to all the NO_x sources in the model. In Figure 4a, up to 95% of the NO_x emission in regions of northern Africa in DJF are from biomass burning. In MAM (Figure 4b) the biomass burning sources in Central America, northern South America, and continental Southeast Asia play a major role, contributing more than 45% to total NO_x emissions in these regions. Biomass burning plays a minor role (< 15%) in the NH during DJF and MAM, with NO_x emissions in the northern midlatitudes predominately a result of fossil fuel combustion. In JJA (Figure 4c), forest fires in Siberia and the Northwest Territories of Canada contribute a significant source of NO_x (> 45%), while at the same time in the SH, northern Australia (> 30%), southern Africa (> 75%), and South America (> 30%) show large percentage contributions from biomass burning. In SON (Figure 4d), significant burning is still taking place in tropical Australia, Africa, and South America.

4. Biomass Burning Impact on CO

The simple chemistry of CO in the model and its relatively long lifetime provides a useful tracer for determining the influence of biomass burning emissions from source regions and the transport of these emissions globally. Data from aircraft measurements, as well as time series from surface observing stations, are available across the globe. The relatively large amount of reliable CO data makes it possible to evaluate the simulated global distribution of CO and, in regions where biomass burning is a major source of CO, to directly assess the reliability of both the magnitude of the biomass burned and CO emitted, as well as the timing of the source.

4.1 Results

The seasonal percent contribution of biomass burning for DJF and JJA are shown in Figures 5a - 5d, as simulated by the GCTM CO experiments. Biomass burning contributes between 15 - 30% to the background CO concentrations throughout most of the troposphere. In DJF (Figure 5a) at the surface, biomass burning contributes up to 80% of the CO over Africa between the equator and 10°N, where the CO concentrations are on average 200 to 300 ppbv. Similar CO concentrations are found over India, where biomass burning contributes up to 60% of the CO in the region. Although the fractional impact on east Asia is similar to India, with up to 60% of CO from biomass burning, the CO concentrations in this region are higher, averaging over 300 ppbv. At the surface, emissions from biomass burning are transported westward in winter monsoon flow from Asia, and from Africa to South America in surface easterlies. At 500 mbar (Figure 5b), CO emissions from biomass burning comprise 30 to 45% of the total CO over Africa, India, and China, and a plume is shown to extend across the Pacific Basin. North of 20°N in Africa, and over South America, CO concentrations between 100 and 200 ppbv at 500 mbar are normally seen in DJF.

In JJA (Figure 5c) the CO distribution shows a major biomass burning contribution over southern Africa (0° to 40°S), In-

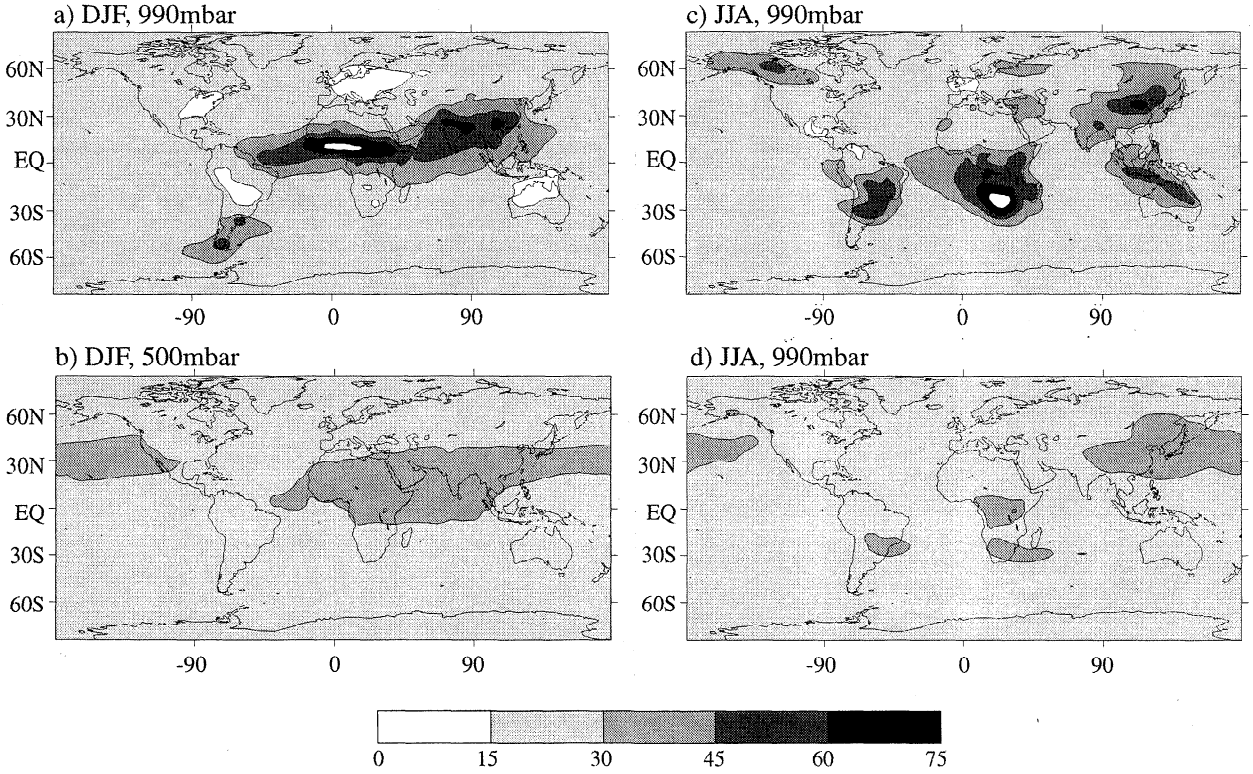

Figure 5. Percent contribution of biomass burning to total CO (white within black denotes values greater than 75%) averaged over (a) December, January, and February (DJF) at 990 mbar, (b) DJF at 500 mbar, (c) June, July, and August (JJA) at 990 mbar, and (d) JJA at 500 mbar.

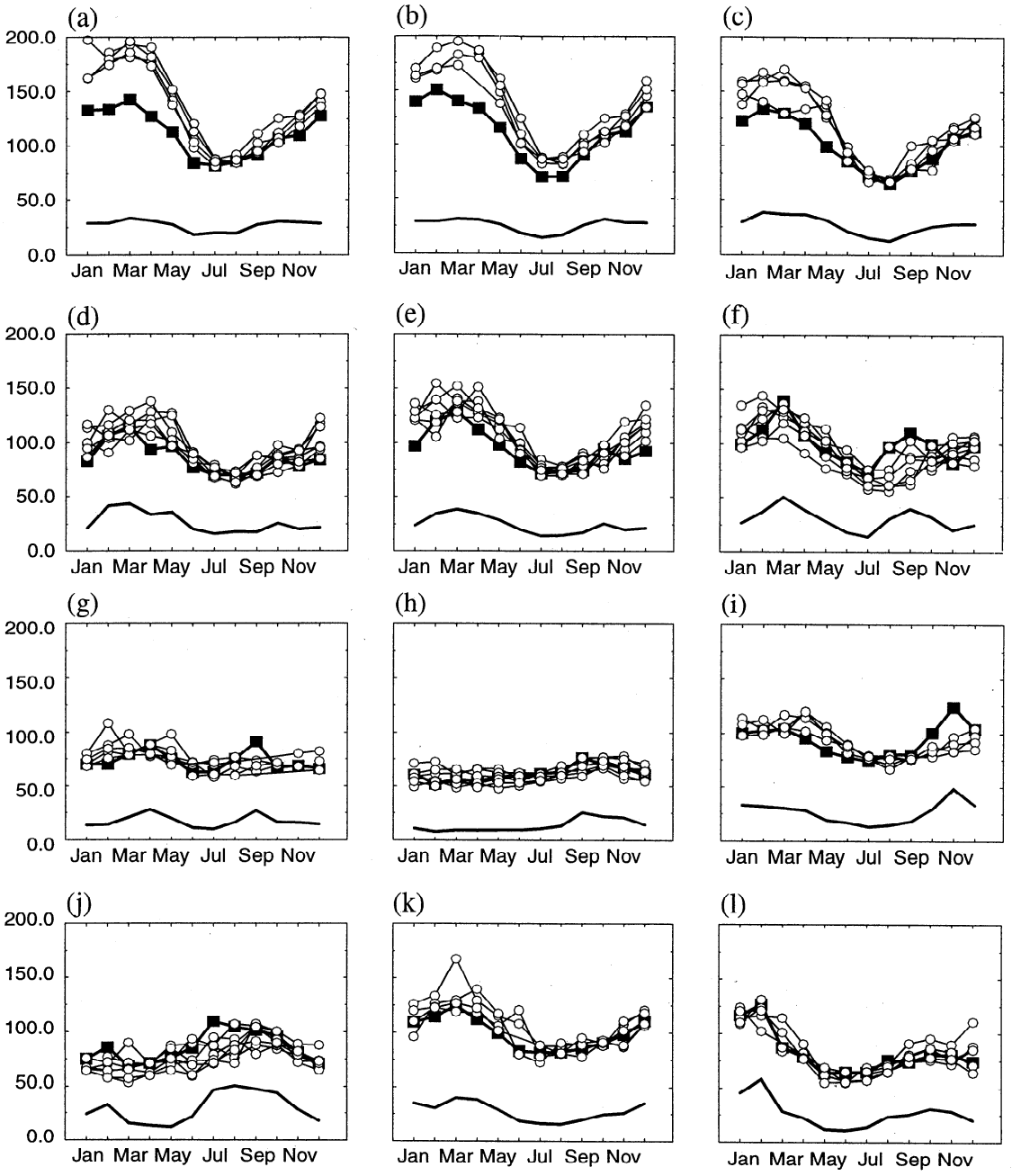

Figure 6. Timeseries data from CMDL tropical stations compared with model results, all in units of ppbv CO. Open circles, measurements; solid squares, model simulation with all sources; solid line, CO from biomass burning only. (a) Mould Bay, Canada; (b) Alert, Canada; (c) Sand Island, Midway; (d) Mauna Loa, Hawaii; (e) Cape Kumukahi, Hawaii; (f) Guam, Marina Islands; (g) Christmas Island; (h) Tutūila, American Samoa; (i) Ragged Point, Barbados; (j) Ascension Island; (k) Tenerife, Canary Islands; (l) Mahe Island, Seychelles.

donesia, northern Australia, Brazil, northern China, and the Northwest Territories of Canada. The most dominant signal at the surface is again over Africa, with over 75% of the CO over South Africa from biomass burning. Australia, Indonesia, Brazil, and the Northwest Territories see contributions of up to 60% CO from the burning. At 500 mbar (Figure 5d), a signal of up to 45% CO from biomass burning is seen again, with a plume from Asia (between 30°N and 60°N) extending across the Pacific Ocean. Plumes with contributions of 30 to 45% from biomass burning also occur over Africa and the lower Brazilian Cerrado.

4.2 Evaluation

As noted, the simulated CO distribution agrees well with both surface observations and aircraft measurements throughout the globe. Holloway et al.'s (submitted manuscript, 1999) work compares with 33 CMDL stations that measured CO and with observations taken at the Jungfraujoch observatory station of the EMPA, with a breakdown of the contributions from each of the CO sources. We now examine more closely observations taken at stations in tropical regions and the boreal forests, where biomass burning plays a dominant role in CO

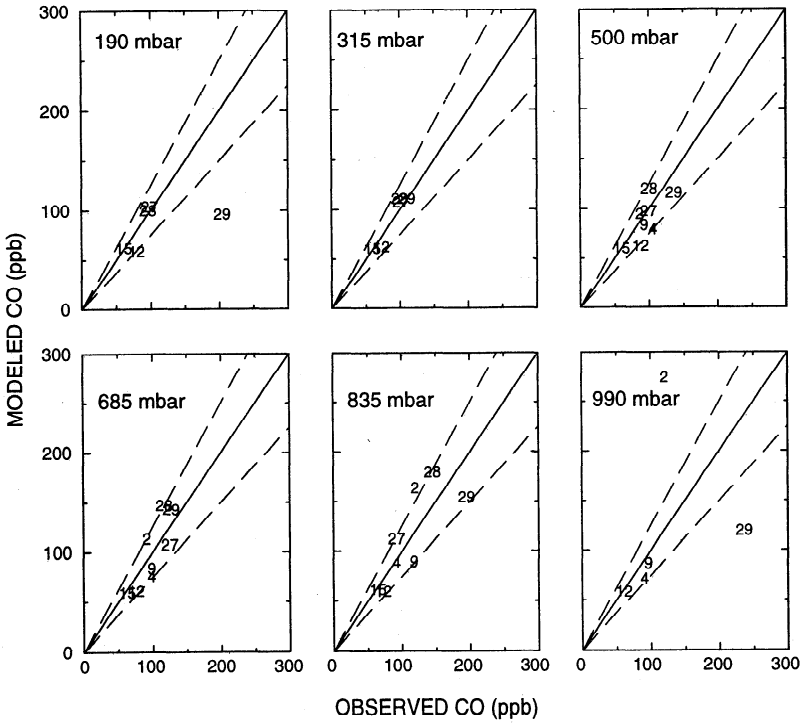

Figure 7. Tropical aircraft CO data from the NASA Global Tropospheric Experiment compared with model CO data. Numbers indicate regions as shown in Table 4 of this paper. Dashed lines represent ±25%.

emissions, to help evaluate the accuracy of the CO source. Figures 6a - 6l show a comparison of the model data (squares) to surface observations (open circles), as well as a time series of the contribution of only biomass burning to the total simulated CO (solid line) at 12 CMDL stations. Monthly mean observations are shown for all years that measurements were taken at each station, rather than as a mean and standard deviation over all years combined. This approach was used as it is a more appropriate comparison to the model's monthly means since the GCTM contains only one representative year of meteorology.

At the NH high-latitude stations of Mould Bay and Alert, Northwest Territories, Canada (Figures 6a and 6b), neither total CO, which fossil fuel emissions dominate, nor the CO seasonal cycle, which is largely determined by large-scale transport of CO to the high latitudes and the concentrations of hydroxyl radicals, are directly controlled by local emissions (Holloway et al., submitted manuscript, 1999). However, in comparison to the observations, the summertime contribution from high-latitude forest fires appears to be reasonable and certainly not too large. Biomass burning emissions contribute to the seasonality at Midway (Figure 6c), Mauna Loa (Figure 6d), Cape Kumukahi (Figure 6e), Tutuila (Figure 6h), Tenerife (Figure 6k), and Mahe Island (Figure 6l), and the model agrees very well with the observations. While agreement is generally good, high CO levels simulated in autumn at Christmas Island (Figure 6g) and Ragged Point (Figure 6i), and in February and July at Ascension Island (Figure 6j), appear to be the result of transport of CO from biomass burning regions. In particular, the November maximum simulated at Ragged Point, Barbados, is from biomass burning emissions transported from the northern Sudan/Sahel region of Africa. Overall the magnitude and timing of the biomass burning source are reasonable in comparison to ground-based observations in regions where biomass burning emissions play an important role in total CO.

Measurements of CO from aircraft campaigns in regions where biomass burning emissions are important also show good agreement with model results. In Figure 7, scatterplots are shown for eight tropical flights of the 10 NASA GTE aircraft campaigns analyzed by Holloway et al. (submitted manuscript, 1999). The numbers refer to the regions listed in Table 4 below (see *Klonecki* [1998] for a discussion of these regions). No systematic bias is seen in the comparison, with almost all of the datapoints falling within ±25% error bounds (dashed lines). The model underestimates CO concentrations at both 190 and 990 mbar in region 29 over eastern South America, measured as part of the TRACE-A campaign. One portion of one flight during TRACE-A made measurements at 190 mbar directly in an outflow region of a cumulus tower [*Fishman et al.*, 1996], and these observations may not be representative of normal CO levels. The high-CO level simulated at the surface of region 2 (Amazon Basin) is the result of the timing of strong regional biomass burning in our source, while the aircraft campaign (Atmospheric Boundary Layer Experiment, ABLE 2A) took place from the early to middle phases (July 18 to August 12) of the 1985 dry season before significant burning in the region. As shown by *Sachse et al.* [1988], CO concentrations increased greatly due to biomass burning in August 1985, and the observations of *Crutzen et al.* [1985], which extended later into the dry season than ABLE 2A, suggest that this increasing trend continues over the entire dry season.

Although uncertainties in timing and magnitude of the source exist, comparison with observations suggest that both our magnitude of biomass burned and CO emitted are reason-

Table 4. Tropical Aircraft Measurement Regions for Which Model Data Are Compared.

Region	Campaign	Longitude	Latitude	Month
2	ABLE 2A	70°W - 45°W	8°S - 2°N	July - Aug.
4	ABLE 3A	175°W - 105°W	50°N - 80°N	July - Aug.
9	CITE 3	35°W - 26°W	11°S - 3°N	Aug. - Sept.
12	PEMtropics A	170°E - 160°W	50°S - Equator	Aug.
15	PEMtropics A	160°W - 120°W	25°S - Equator	Aug.
27	TRACE-A	12°E - 40°E	35°S - 10°S	Sept. - Oct.
28	TRACE-A	20°W - 10°E	20°S - Equator	Sept. - Oct.
29	TRACE-A	55°W - 35°W	30°S - 5°S	Sept. - Oct.

ABLE 2, Atmospheric Boundary Layer Experiment; CITE 3, Chemical Instrumentation Test and Evaluation; PEMtropics A, Pacific Exploratory Mission; TRACE-A, Transport and Atmospheric Chemistry Near the Equator - Atlantic.

able. The simulation clearly captures seasonal changes in the observed CO concentrations. A doubling of the biomass burning source would uniformly produce overestimations of total CO in the tropics. Similarly, halving the CO biomass burning source would result in uniform underestimations, particularly at stations where biomass burning plays a dominant role in total CO (see Figure 6a - 6l). The magnitude of the biomass burning also compares well with recent annual estimates of biomass burned in the tropics as shown in Table 5, assuming the emission factors used to convert the GCTM biomass burning source into teragrams of biomass are reasonable (45% carbon content in dry biomass [*Andreae*,1991]). Savannas are the major source of biomass burning in the tropics in our source, in agreement with *Andreae* [1991], *Hao and Liu* [1994], and J.A. Logan and R. Yevich's estimates as reported by *Lobert et al.* [1999]. The "tropics" estimates found in Table 5 for our source are calculated based on the areas covered by *Hao and Liu*'s [1994] database plus Australia. Globally, J.A. Logan and R. Yevich's source contains much less forest burning than estimated in our source. Much of the difference in these estimates lies outside of the tropics and thus mainly in the boreal forest areas where we assume the biomass is only forest for budget calculations. In addition, J.A. Logan and R. Yevich's source features much more fuelwood burning than found in our source; however, their estimates include charcoal burning. The range in previous estimates for the magnitude of burning in the tropics is from 3260 to 10,450 Tg of biomass, suggesting a large range of error. Based on comparison with other estimates and CO observations, we believe that the uncertainty in our current estimates of both global biomass burning and the resulting global CO source, as well as the regional magnitudes and timing, are much less than the factor of 2 suggested above.

5. Biomass Burning Impact on Nitrogen Oxides (NO_x)

NO_x ($NO+NO_2$) has long been known to play an important role in tropospheric ozone production [*Chameides and Walker*, 1973; *Crutzen*, 1974] and to impact OH concentrations, linking NO_x to the oxidizing efficiency of the troposphere. Recent analyses have demonstrated NO_x control of ozone production throughout much of the free troposphere [e.g., *Klonecki and Levy*, 1997].

5.1 Results

Figures 8a - 8d depict the simulated seasonal percent contributions of biomass burning emissions of NO_x to total NO_x concentration at the surface and 500 mbar for DJF and JJA. Impacts are only considered where total NO_x is greater than 20 pptv because concentrations less than this do not allow significant O_3 production [*Klonecki and Levy*, 1997]. As shown in Figure 8a, more than 75% of the NO_x at the surface near equatorial Africa is a result of biomass burning during DJF. The mixing ratios over equatorial Africa are generally greater than 1 ppbv, reaching just above 3 ppbv along the Ivory Coast. There is also a large contribution over Tierra del Fuego at the surface, where NO_x mixing ratios are less than 1 ppbv; $HINO_3$

Table 5. Comparison of Various Estimates of Amount (Teragrams) of Biomass Burned in the Tropics and Globally.

	Seiler and Crutzen [1980] (Tropics)[a]	Crutzen and Andreae [1990] (Tropics)[a]	Andreae [1991] (Tropics)[a]	Hao and Liu [1994] (Tropics)[a]	This Work (Tropics)[b]	This Work (Global)	Logan and Yevich (Global)[c]
Forest[d]	1450-3380	1550-3780	1260	1820	1497	2821	1915
Savanna	480-1900	670-3560	3690	2670	2343	2720	3133
Fuelwood	620	670-1330	1260	620	608	838	1946[c]
Agricultural residues	710	1110-1780	1360	280	296	296	475
Domestic residues					183	585	718[c]
Dung					95	118	
Shrub and grasslands							71
Total	3260-6610	4000-10450	7570	5390	5022	7378	8258

[a] Values represent tropical estimates only (*Hao and Liu* [1994]).

[b] Tropics as defined by database of *Hao and Liu* [1994] plus Australia.

[c] Global estimates as reported by *Lobert et al.* [1999] and based on conversion factor from Tg C/yr of 0.45; Logan and Yevich's "fuelwood" estimates include charcoal burning, and "domestic residues" include dung.

[d] Value includes deforestation and shifting cultivation.

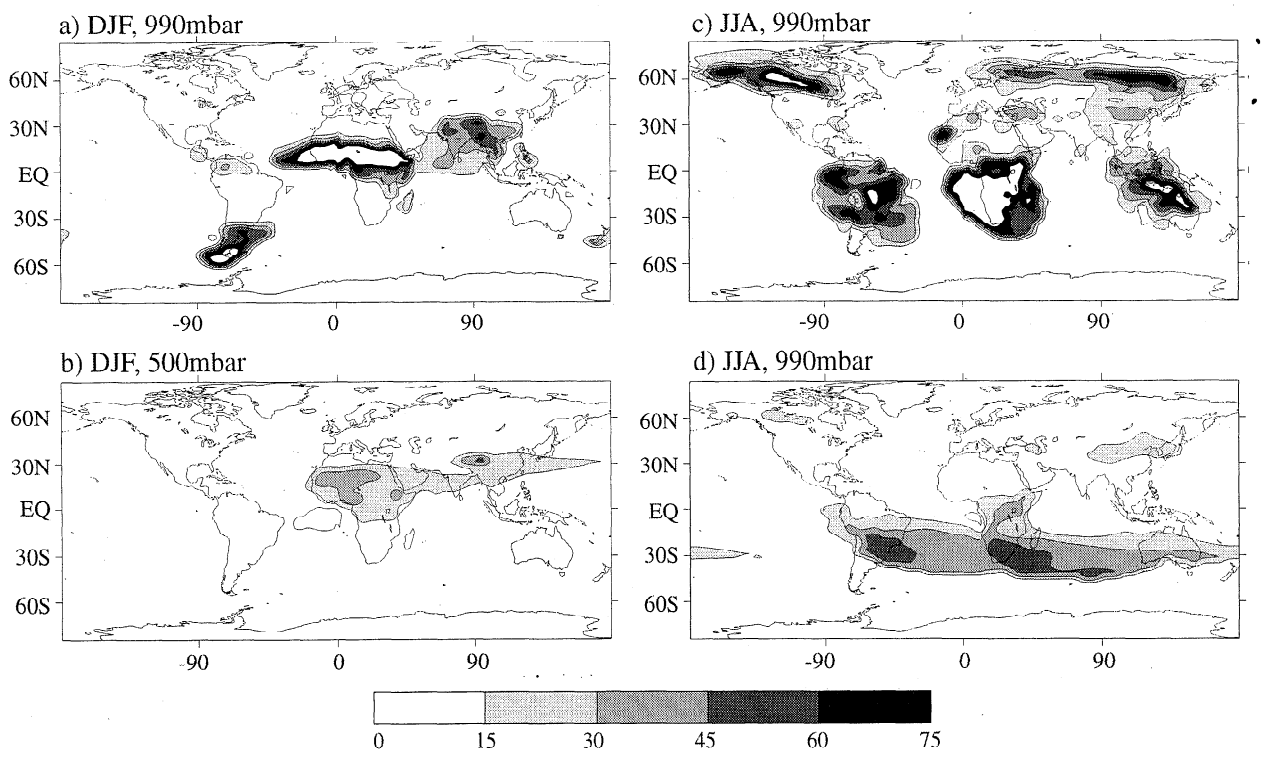

Figure 8. Percent contribution of biomass burning to total NO_x (impacts only considered where NO_x concentration is > 20 pptv; white inside black indicates values greater than 75%) averaged over (a) December, January, and February (DJF) at 990 mbar, (b) DJF at 500 mbar, (c) June, July, and August (JJA) at 990 mbar, and (d) JJA at 500 mbar.

wet deposition measurements at Torres de Paine (52°S, 73°W) show reasonable agreement with model data [see *Levy et al.*, 1999, Figure 3d]. The smaller percent contribution seen over China and India, in comparison to Africa, is the result of two factors: first, the maximum in the burning season for Southeast Asia occurs in March, and second, Asia has a much larger source of NO_x from fossil fuel combustion than equatorial Africa. At 500 mbar (Figure 8b), transport of NO_x from biomass burning in Africa and Asia stretches into the Pacific Ocean. Throughout the tropics, NO_x mixing ratios at this level range from 0.05 to 0.2 ppbv over land. Figures 8c and 8d show the percent contribution of NO_x emissions from biomass burning averaged over JJA at the surface and 500 mbar. At the surface, southern Africa is at the height of its burning season and the burning contributes over 75% of total NO_x. This season also provides dry conditions conducive for burning in the Brazilian Cerrado, Amazon Basin, Indonesia, and northern Australia, where average NO_x mixing ratios are found to be greater than 1 ppbv during this time of year. At 500 mbar, emissions of NO_x from biomass burning are transported throughout the SH, with plumes stretching off of South Africa and South America. The NH only sees significant contributions from biomass burning (30 - 45%) at this level, over Asia and the Northwest Territories of Canada. For both seasons the contribution of biomass burning to NO_x at 190 mbar (not shown) drops off to less than 15% across most of the globe. Throughout the year, lightning becomes the dominant (50% or more) source of NO_x between 30°N and 30°S at 500 mbar and above (see *Levy et al.* [1999, Figure 10]). While there still exists significant uncertainty in the absolute magnitude of the lightning source (see section 5 of *Levy et al.* [1999] for a detailed discussion), it does not significantly influence the role of biomass burning. The one exception to lightning dominance in the upper half of the tropical troposphere is the July-October plume of biomass burning NO_x stretching off of South Africa and South America between 20°S and 40°S at 500 mbar, which accounts for up to 50% of the NO_x in that region (Figure 8d).

5.2 Evaluation

In comparing simulated NO_x concentrations with observations from the aircraft campaign regions listed in Table 4, the model shows no systematic bias, with 92% of the datapoints falling within ±50% of the 1:1 line (see *Levy et al.* [1999, Figure 6] for details). As for CO, the model underestimates the measured values of NO_x in region 29 (TRACE-A) at 190 mbar. Simulated NO_y (NO_x+HNO_3+PAN) also agrees well with measurements from these same aircraft campaigns (over 95% within ±50% error limits) [see *Levy et al.*, 1999, Figure 5]. In addition, the model generally captures the observed spatial patterns and magnitudes of wet deposition of HNO_3 in biomass burning source regions, with 71% of datapoints from 21 observation sites falling within ±50% (see *Levy et al.* [1999, Figure 3]).

General uncertainties in our biomass burning source are discussed in section 7 below. While the NO_x observations are much more sparse than for CO and the comparisons between observations and model show more scatter, there is no systematic bias. The increased discrepancies in NO_x may be explained by its much shorter lifetime in comparison to CO, and its greater sensitivity to local errors in timing, magnitude of burning and emission factors. Again, however, either a uni-

form doubling or halving of the NO_x biomass burning source would generate unreasonable results through most of the tropical lower troposphere. As is in the case of the CO source, the uncertainty in the magnitude of the global NO_x biomass burning source is less than a factor of 2. However, the OH fields used for the NO_x simulation, which directly effect the NO_x lifetime and the resulting long-range impact of the biomass burning emissions, have a methyl chloroform lifetime of 6.3 years. The 30% increase in OH needed to reduce the lifetime to 4.8 years would also reduce the long-range impact of the biomass burning NO_x. This does suggest that our simulated impact of biomass burning on NO_x in the more remote free troposphere is an upper bound.

6. Biomass Burning Impact on Ozone (O_3)

While biomass burning does not directly produce tropospheric O_3, it is a significant contributor to important precursors of O_3, namely, NO_x and CO. To assess the contribution of biomass burning to NO_x and CO, the experiments are run without any burning and then subtracted from the full source simulation to minimize numerical nonlinearities in transport. While biomass burning emissions add directly to NO_x and CO, their resulting impact on O_3 is buffered by the nonlinear response of the coupled ozone chemistry and transport. Therefore, to evaluate the effects of biomass burning on O_3 concentrations, an O_3 simulation, which uses NO_x and CO fields generated without biomass burning emissions, is compared to an O_3 simulation using CO and NO_x fields generated with all sources.

6.1 Results

Figures 9a - 9h depict the average seasonal percent contribution of biomass burning to the simulated O_3 concentrations near the surface and 500 mbar for DJF, MAM, JJA, and SON. As expected, the predominant effect on O_3 is in the tropical regions of Africa, South America, Australia, and Indonesia, where biomass burning had the largest impact on CO and NO_x. The largest influence of biomass burning on O_3 during all four seasons is at the surface (Figure 9a), where NO_x and CO are directly produced by the source. In general, at 940 mbar, mixing ratios throughout the NH range between 25 and 50 ppbv, while the SH is covered in mixing ratios between 10 and 25 ppbv, with a minimum occurring over the equatorial Pacific Ocean. In DJF (Figure 9a), biomass burning contributes 30 to 40% to the O_3 concentrations over equatorial and northern Africa at 940 mbar, while the influence over southern South America is between 10 and 20%.

During MAM (Figure 9b), plumes impacted up to 30% are seen over Central America, northern South America, Africa, and Southeast Asia. The impact on O_3 over continental Southeast Asia is largest during this time of year. Significant impacts are seen in NO_x and CO in this region during MAM, with biomass burning contributing up to 75% of total NO_x over land and up to 60% of total CO concentrations. *Liu et al.* [1999] hypothesize that biomass burning in Southeast Asia provide enough precursors to result in ozone enhancements between February and April over Hong Kong, based on observed humidity levels and backtrajectory analysis. Our results are consistent with this hypothesis showing a 10 to 15 ppbv enhancement in the lower and midtroposphere over Hong Kong due to biomass burning in the region. During the NH spring, the model results show mixing ratios up to 80 ppbv at the 685-mbar level and up to 90 ppbv at the 500-mbar level but do not exhibit increases in the lower troposphere as large as in the events described by *Liu et al.* [1999].

During JJA (Figure 9c), the boreal forest fires of Siberia and the Northwest Territories contribute 10 to 20% of the O_3 produced in those regions. In the tropics, more significant influences (> 20%) of biomass burning are seen over Indonesia, Africa, and northern South America. In JJA the largest signal is again seen over Africa, with biomass burning contributing up to 30 to 40% of the O_3 near the equatorial region of the continent.

Large impacts on O_3 are seen in SON (Figure 9d) over Africa, Indonesia, northern Australia, and the Brazilian Cerrado region with biomass burning contributing between 30 and 40% to O_3. Transport of impacted air is seen throughout the Southern Hemisphere, contributing between 10 to 20%. *Schultz et al.* [1999] show that in the Harvard/Goddard Institute for Space Studies three-dimensional model, biomass burning increases average ozone concentrations by 7 - 8 ppbv throughout the troposphere. They report average ozone mixing ratios for September in the tropical South Pacific as 31 ppbv in the lower troposphere (0 - 4.5 km) and 44 ppbv in the upper troposphere (4.5 - 13 km). Our work, which is in general agreement, finds ozone mixing ratios for the same region in September of 29 ppbv in the lower troposphere and 51 ppbv in the upper troposphere, with biomass burning contributing 4 - 5 ppbv O_3 in the boundary layer and 6 ppbv uniformly in the free troposphere. Although the absolute contribution of biomass burning to O_3 is similar throughout the troposphere in this region and falls within the 10 to 20% range in both Figures 9d and 9h, its percentage contribution decreases with height. Figure 9d also shows part of Indonesia with impacts of 40 to 50% (and slightly over 50%) on O_3 concentrations. Throughout the year the background NO_x concentrations are generally lower in Indonesia than Africa and South America. The Indonesian archipelago air quality is moderated by the influence of NO_x- and O_3-poor air from the ocean, in comparison to the continental biomass burning regions. This causes the atmosphere near Indonesia and northern Australia to be more sensitive to fluctuations in NO_x concentrations, and thus biomass burning has a larger influence on O_3 concentrations in the region. In general, across the globe the largest impacts on O_3 during all four seasons are limited to source regions, due to the larger NO_x concentrations in these areas.

Figures 9e - 9h present the seasonal contributions of biomass burning to O_3 at 500 mbar for all four seasons. On the average, O_3 mixing ratios in the NH at this level are between 50 and 75 ppbv, while in the SH they range between 25 and 50 ppbv. The dominant effect of biomass burning is seen over Africa, contributing 10 to 20% to the simulated O_3 during DJF, MAM, and JJA, and over 20% in SON. During SON, biomass burning influence (15 to 30%) is seen throughout the SH background O_3 concentrations at 500 mbar.

In the upper troposphere (not shown), the influence of biomass burning is much less during all four seasons, with minor contributions occurring over regions of deep convection. Most of the O_3 occurring at this level is either from stratospheric input in the extratropics or the result of chemical production driven by lightning NO_x in the tropics.

6.2 Evaluation

Several workers have developed methods for deriving tropospheric column ozone from satellite observations [e.g.,

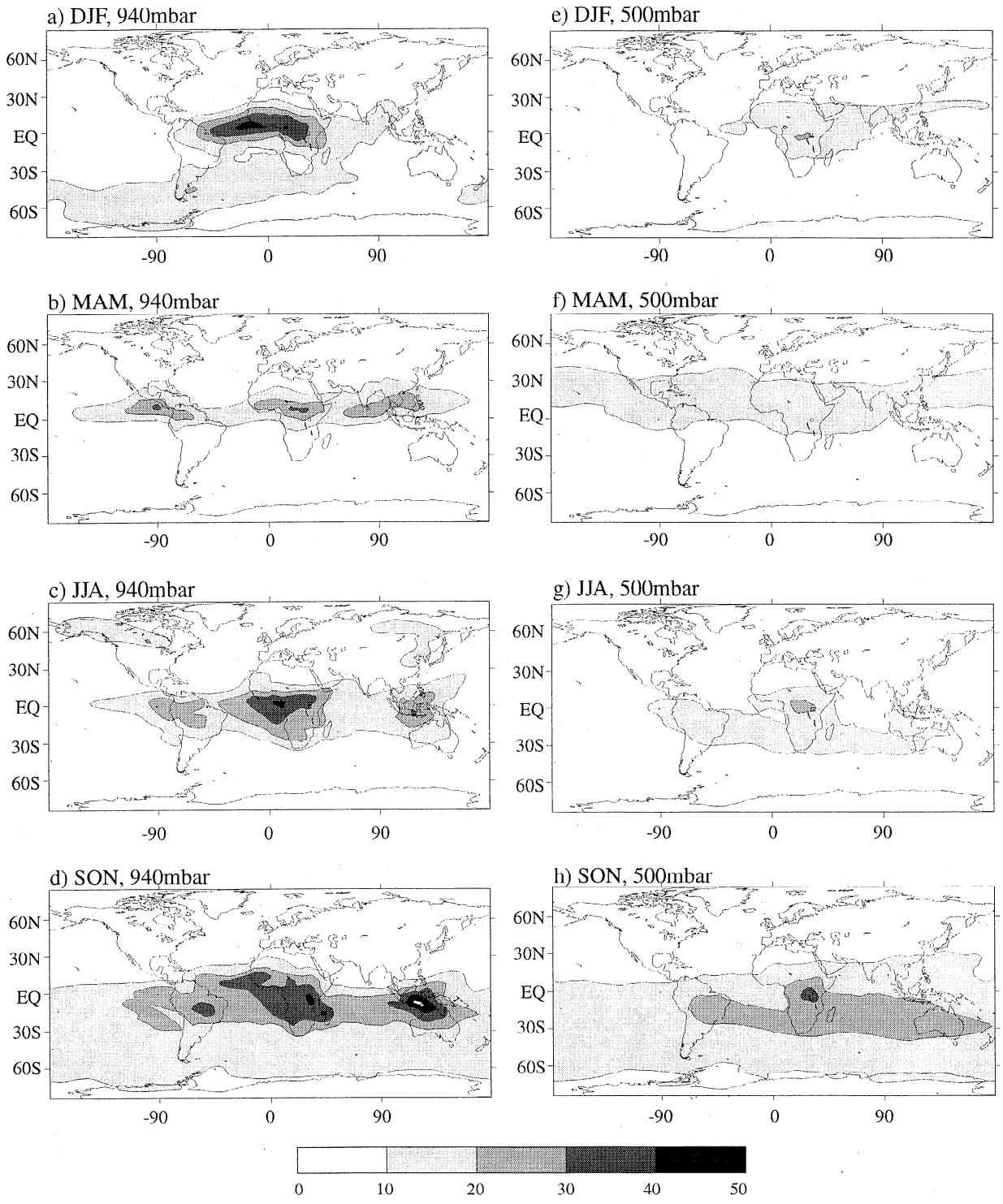

Figure 9. Percentage contribution of biomass burning to simulated O_3 distribution at 940 mbar for (a) December, January, February (DJF), (b) March, April, May (MAM), (c) June, July, August (JJA), and (d) September, October, November (SON), O_3 distribution at 500 mbar for (e) DJF, (f) MAM, (g) JJA, and (h) SON.

Hudson and Thompson, 1998; *Ziemke et al.*, 1998; *Kim et al.*, 1996; *Fishman and Brackett*, 1997, and references therein], and despite the differences in the techniques there is general qualitative agreement. The use of tropospheric column ozone has provided insight into the geographic distribution of O_3 and the contributions of O_3 from continental plumes arising from North America, Europe, Africa, and Asia [*Fishman and Brackett*, 1997]. The seasonal distribution of the GCTM's simulated tropospheric column ozone in the tropics is shown in Plates 1a - 1d. Due to the relative coarse vertical resolution of the GCTM, we choose to define air containing ozone mixing ratios of less than 100 ppbv as tropospheric, which typically implies a tropopause of 150 mbar in our model tropics and 240 mbar in the midlatitudes. In order to provide a smooth poleward transition incorporating longitudinal O_3 variations due to transient weather systems, the tropopause is

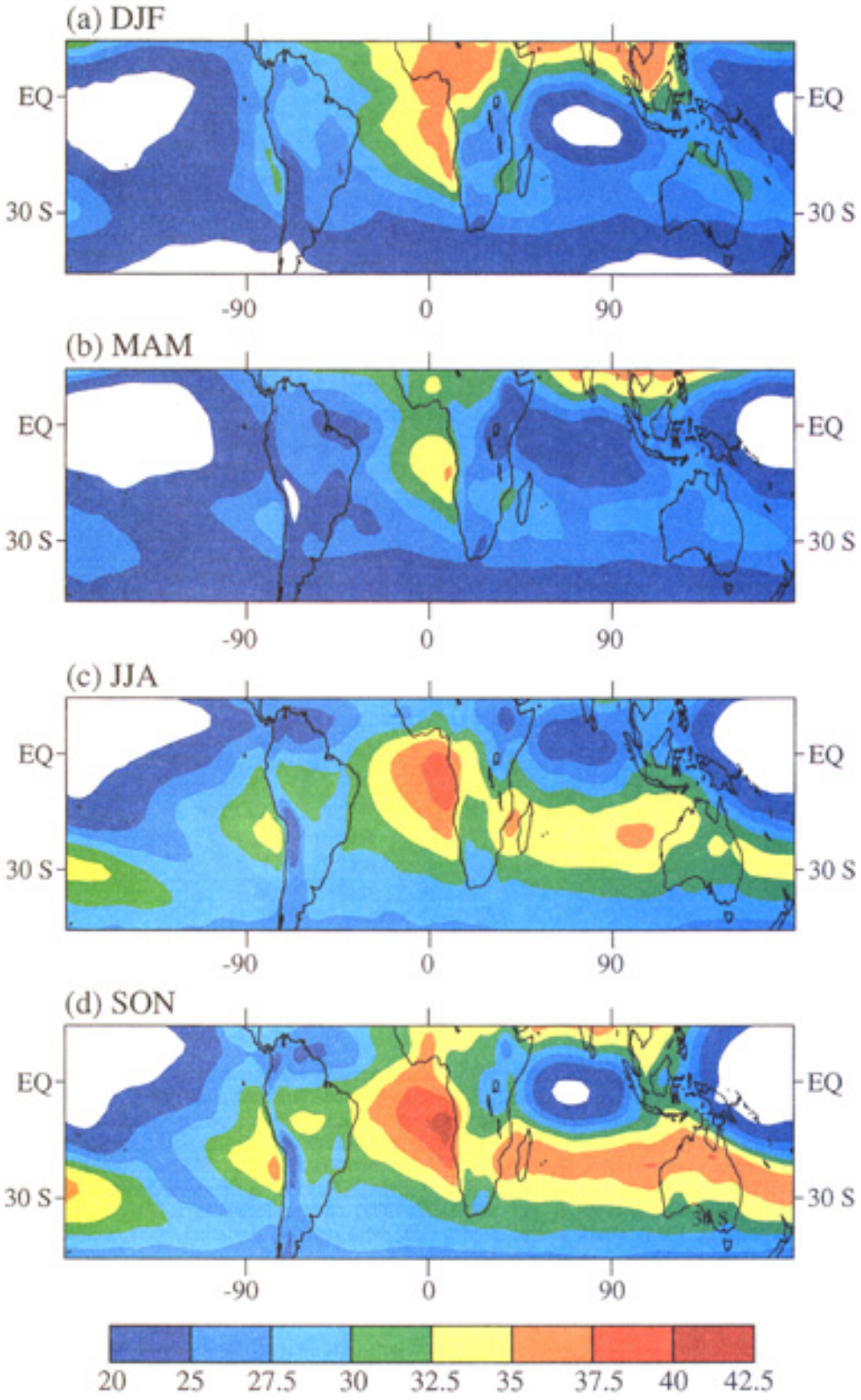

Plate 1. Tropospheric column O_3 in Dobson units (DU) from a model simulation (white within dark blue denotes values less than 20 DU) for (a) December, January, February (DJF), (b) March, April, May (MAM), (c) June, July August (JJA), and (d) September, October, November (SON).

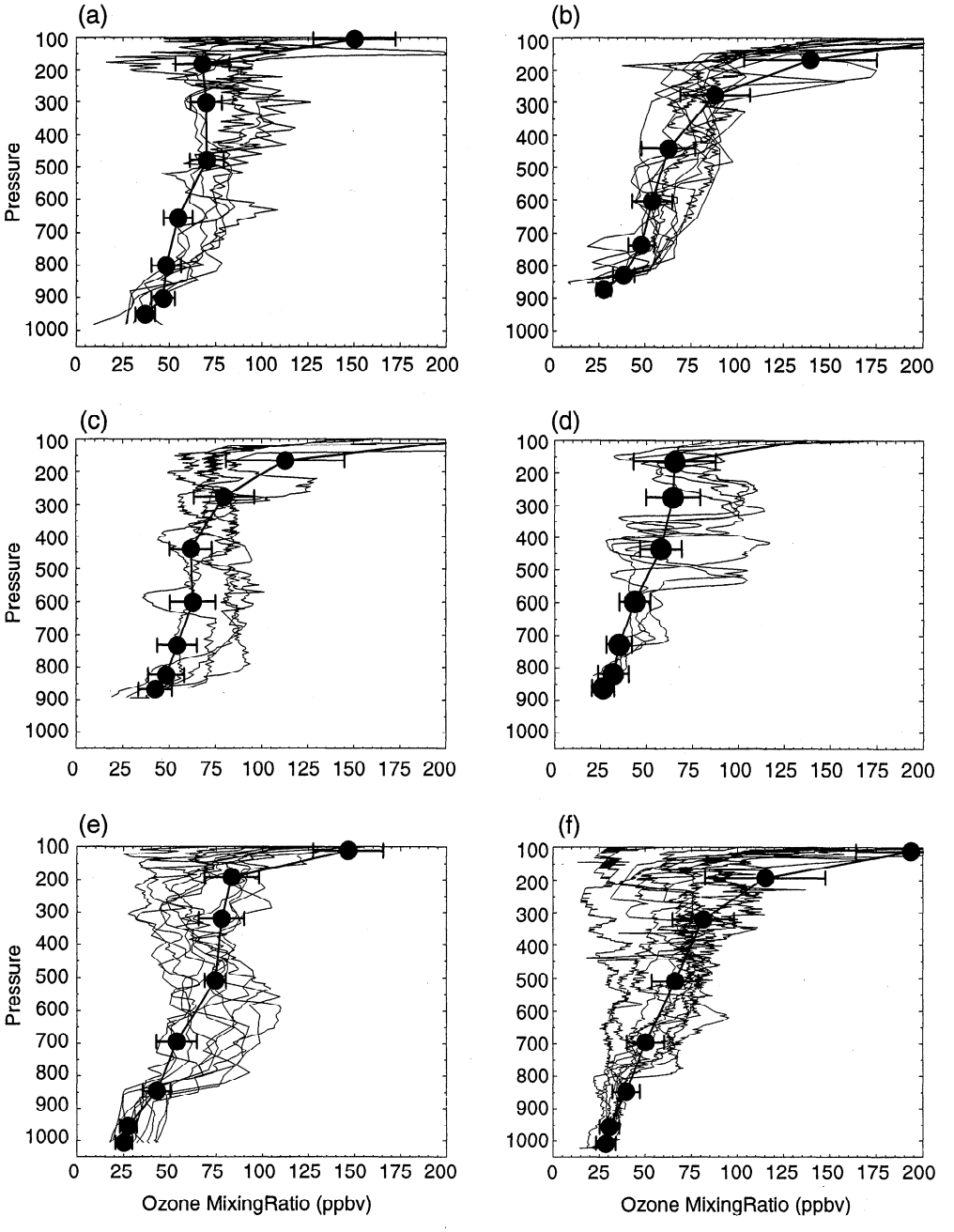

Figure 10. Ozonesondes sites located in the tropics compared with model results: (a) Brazzaville (NASA/GTE data archive at NASA Langley), (b) Irene (J.R. Olson, personal communication, 1998), (c) Etosha (NASA/GTE data archive at NASA Langley), (d) Nairobi (Southern Hemisphere Additional Ozonesondes (SHADOZ), 1999), (e) Ascension Island (NASA/GTE data archive at NASA Langley), (f) Reunion Island (F. Sokolic, personal communication, 1998), (g) Cuiaba (Kirchhoff et al., 1996), (h) Porto National (Kirchhoff et al., 1996), (i) Natal (Kirchhoff et al., 1996), (j) Samoa (SHADOZ, 1999; S. Oltmans, personal communication, 1998), (k) Tahiti (SHADOZ, 1999), (l) Fiji (SHADOZ, 1999), and (m) Pataya Jaya, Malaysia (Malaysian Meteorological Society, 1998). Black circles, model value with standard deviation of September mean value; black lines, individual sondes; **n**, number of ozonesondes.

determined and the tropospheric column ozone is calculated in all grid boxes every 6 hours of model integration. The value of 100 ppbv is somewhat subjective; however, it is based on the examination of numerous ozonesondes, and it ensures that our column lids are always in the troposphere. Additionally, our purpose in comparing with satellite observations of tropospheric column ozone is to provide a qualitative picture of the reliability of the spatial pattern from the simulated vertically integrated ozone concentrations.

In comparing *Fishman and Brackett*'s [1997] seasonal estimates to the GCTM results, the GCTM shows an approximate +5 Dobson units (DU) bias in most of the tropics though major geographical features are still captured. Fishman and Brackett's most recent estimates using the tropospheric ozone

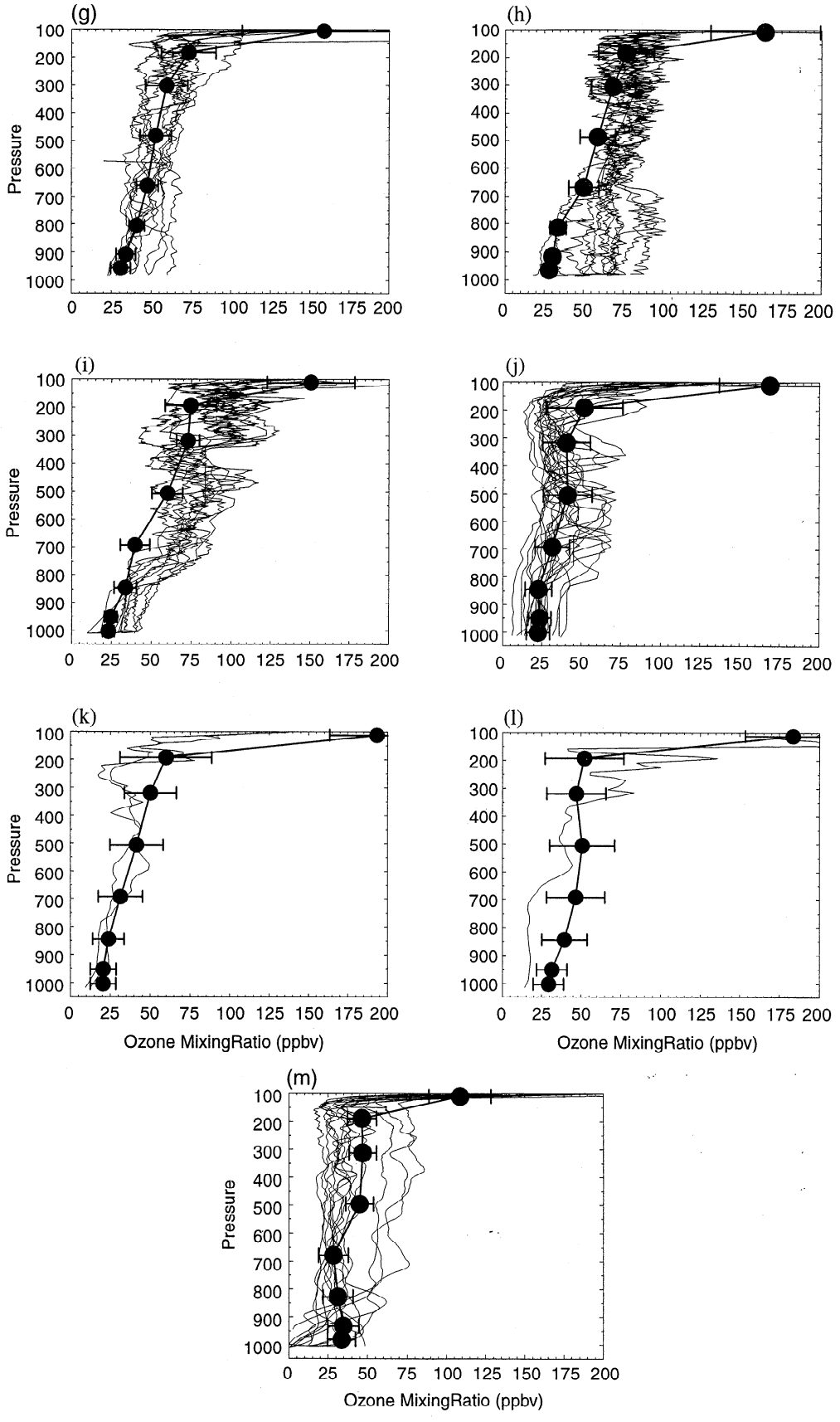

Figure 10. (continued)

residual technique show an average decrease of 5 DU over previous work [e.g., *Fishman et al.*, 1990, 1996]. For instance, in DJF (Plate 1a) the GCTM results show a pattern similar to Fishman and Brackett's in the tropics, with the highest values off of Africa and lowest values in the tropical Pacific Ocean. However, the GCTM results show enhancement of tropospheric column O_3 over northern Africa, an area of significant biomass burning, which does not show up in Fishman and Brackett's analyses. In MAM (Plate 1b), a plume slightly offshore and of higher magnitude (+5 DU) than Fishman and Brackett's latest analysis develops off of southwest Africa. In JJA and SON (Plates 1c and 1d), higher ozone levels are depicted throughout the tropics, corresponding with increases in biomass burning, with transport of ozone from South America, Africa, and Asia throughout the SH. The eastward plume off of Africa occurs slightly north of Fishman and Brackett's depiction, and the large values occurring over the South Atlantic are higher than Fishman and Brackett's estimates, though they agree well with *Ziemke et al.* [1998]. Overall, the major features in tropospheric column ozone are captured in the GCTM simulation and the influence of biomass burning is clearly seen in the seasonally enhanced plumes of O_3.

Again we focus on comparisons with observations taken in regions of significant biomass burning. Figures 10a - 10m present comparisons at 13 tropical sites of model results and observations during September. Data from the following stations are shown: Ascension Island, Brazzaville, Cuiaba, Etosha, Fiji, Irene (Pretoria), Malaysia, Nairobi, Natal, Porto National, Reunion Island, Samoa, and Tahiti, with station location, source of data, and the number of available ozonesondes depicted in the figure. Data collected during September are compared with the model's monthly averaged data (with standard deviation based on averaging over every 6-hour time step in the month), since September is the peak month for burning through most of the Southern Hemisphere.

The model overlaps with most of the data taken at the African stations of Brazzaville, Irene, Etosha, and Nairobi (Figures 10a - 10d). However, at both Brazzaville and Nairobi the significant increase in ozone concentration seen near 650 mbar in the observations, a likely result of biomass burning, is not seen in the model. At Ascension Island (Figure 10e), a biomass burning signal is also seen in the lower free troposphere, as a result of transport from equatorial Africa. The model captures some of this increase at 500 mbar. The model results overlap well with data collected at Reunion Island (Figure 10f). Moving to South America, Cuiaba (Figure 10g) does not exhibit a large increase with height in the vertical profile of O_3 in the troposphere, while at Porto and Natal (Figures 10h and 10i), large increases are seen in the lower and middle troposphere, respectively. At Porto the model overlaps with several ozonesondes but is lower than the majority of measurements taken at this site and would most likely be improved by an increase of the biomass burning source locally. At Natal the model's lack of a large increase in the midtroposphere during September appears to be due to the easterly transport of marine air in the GCTM. A model grid box located three boxes south of Natal (not shown) does show more of an increase at this level due to transport of ozone produced from biomass burning over South America. Moving into the Pacific Ocean, the model is shown to capture the ozone profiles well at Samoa, Tahiti, and Fiji (Figures 10j - 10l), although the data available for the latter two stations are sparse. Finally, the model is compared with ozonesondes taken at Pataya Jaya, Malaysia (Figure 10m). At this location, the model results prove to be higher than most of the observed values. The three anomalously high observed profiles are due to increased burning during September of 1994 and 1997 caused by El Nino induced droughts.

Comparison of model results with O_3 observations shows no systematic errors in the simulated values. The model compares well with the seasonal distribution of total tropospheric column O_3 in comparison to satellite observations. Comparison with ozonesondes at tropical stations show the model reproduces the general trends in the vertical profiles. However, there are specific features, primarily an ozone bulge in the lower free troposphere over Ascension, Brazzaville, and Natal, which are believed to result from biomass burning and are not captured below 600 mbar in the simulation. Simply increasing the biomass burning sources for NO_x and CO does not produce this 800 - 600 mbar bulge, though it would produce the enhanced Porto profiles which increase from the surface to 700 mbar. We believe that this bulge is missing due to inadequate transport, which is probably an effect of the model's resolution. A detailed study is currently being conducted on the ozone maximum occurring off of Africa (see Plates 1a - 1d) and that analysis will discuss these issues in more detail. Overall, the model simulation of O_3 fares well in comparison to observations, and though not perfect, provides a useful and appropriate tool for analyzing the indirect impacts of biomass burning on O_3 concentrations regionally and globally.

7. Summary of Uncertainty in Biomass Burning Emissions

Uncertainty in the biomass burning sources lies in three key areas: timing, overall mass burned, and emission factors applied to the biomass burned. The first of these, the timing of biomass burning, is perhaps the easiest to verify because of the data available from satellite monitoring. In addition, comparison with observations from long-term monitoring stations show reasonable agreement with the GCTM's seasonal signals of NO_x and CO.

The second area of uncertainty, the amount of biomass burned, is largely due to a lack of data, and in some cases a lack of reliable data on land use practices and aboveground biomass density. In comparing our new biomass burning sources to previous estimates of biomass burned annually in the tropics, we find our estimate well within the published range of 3260 to 10,450 Tg of biomass burned (see Table 5). Our sources include savanna fires as the predominant source of biomass burning in the tropics, in agreement with *Andreae* [1991], *Hao and Liu* [1994], and J.A. Logan and R. Yevich's estimates as reported by *Lobert et al.* [1999].

The third and perhaps most uncertain part of the biomass burning source lies in the use of uniform emission factors for all biomass types, except for the biofuels in Asia [*Streets and Waldhoff*, 1998]. While the general agreement with observations of CO, NO_x, and O_3 suggests that this effect may be small, it could be improved.

As mentioned, previous estimates of biomass burned suggest a large range in error. Based on this it could be assumed that a large error exists in our estimates. However, the agreement between simulated and observed CO in the tropics suggests that our seasonal estimates of biomass burned, both globally and regionally, are more tightly bound than Table 5

might suggest. Thus we believe the CO global biomass burning source proves certain to much less than a factor of 2. Time series comparisons at long-term monitoring stations where biomass burning plays a dominant role show that general trends in the seasonal distribution of CO are captured. This further suggests that the magnitude and timing of the biomass burning sources is reasonable at a regional level based on monthly averages of burning. This conclusion is supported by comparison with NO_x and O_3 data as well, although there is much less data available for these species than for CO.

More NO_x and O_3 data, particularly in regions where biomass burning is predominant, will allow for further detailed studies of biomass burning impacts on atmospheric chemistry. Additional long-term monitoring stations and more readily available data in regions like South and Central America and tropical Asia will also certainly help in this continued effort.

8. Conclusions

Biomass burning contributes to more than 50% of both the NO_x and CO in the boundary layer over major source regions, while indirectly contributing up to half of the O_3 concentrations over major tropical burning regions. In comparison to NO_x and O_3, biomass burning has the largest global impact on the CO distribution, contributing 15 to 30% to the entire global tropospheric CO background. As expected, based on previous studies, the most significant impacts from biomass burning emissions occur in the tropical lower troposphere. Due to the shorter lifetime of NO_x, emissions of NO_x from biomass burning have the most significant impact over source regions; since NO_x plays a direct role in O_3 production, major impacts on O_3 are also limited to source regions. Near the surface, biomass burning indirectly contributes more than 15% of the total O_3 concentrations in the tropics throughout the year, and 10 to 20% throughout the Southern Hemisphere during SON. Biomass burning does not contribute significantly to either NO_x or O_3 in the upper troposphere.

Comparisons with a significant number of reliable ground-based and aircraft CO data provide a useful diagnostic of the biomass burning source used in the model. Although data are less abundant for NO_x and O_3, comparisons with model results shows reasonable agreement in major biomass burning regions. The total tropospheric column O_3 distribution in the tropics is also in reasonable agreement with recent estimates based on satellite observations [e.g., *Hudson and Thompson*, 1998; *Ziemke et al.*, 1998; *Kim et al.*, 1996; *Fishman and Brackett*, 1997]. The model shows reasonable profiles in comparison to ozonesondes taken in the tropics and generally captures seasonal changes in O_3 concentrations caused indirectly by biomass burning. Based on agreement with observations and previous estimates of biomass burned in the tropics annually, we conclude that the uncertainties in our biomass burning sources of CO and NO_x are much less than the a priori factor of 2 implied by previous estimates.

Acknowledgments. We wish to acknowledge the continuous support and effort on the part of Bud Moxim, and the useful comments of David Baker, William Cooke, Tracey Holloway, and two anonymous reviewers. We also thank Jennifer A. Logan, Sam Oltmans, Johann Goldammer, Jennifer Richardson Olson, and Mahesh Phadnis for their advice and sharing of information; and Sarath Guttikunda for his work in support of this manuscript. In addition, we wish to thank Lim Joo Tick of the Malaysian Meteorological Society. M.K.G. wishes to thank the Center for Global and Regional Environmental Research at the University of Iowa for support through NASA grant G-35-W21-G2 and the Atmospheric and Oceanic Sciences Program at Princeton for support from NOAA grant NA67RJ0120.

References

Andreae, M.O., Biomass burning: Its history, use, and distribution and its impact on environmental quality and global quality, in *Global Biomass Burning: Atmospheric, Climatic, and Biospheric Implications*, edited by J.S. Levine, pp. 3-21, MIT Press, Cambridge, Mass., 1991.

Andreae, M.O., et al., Biomass-burning emissions and associated haze layers over Amazonia, *J. Geophys. Res.*, *93*, 1509-1527, 1988.

Chameides, W.L., and J.C.G. Walker, A photochemical theory of tropospheric ozone, *J. Geophys. Res.*, *78*, 8751-8760, 1973.

Chameides, W.L., P.S. Kasibhatla, J.J. Yienger, H. Levy II, and W.J. Moxim, The growth of continental-scale metro-agro-plexes, regional ozone pollution, and world food production, *Science*, *264*, 74-77, 1994.

Cooke, W.F., B. Koffi, and J.-M. Gregoire, Seasonality of vegetation fires in Africa from remote sensing data and application to a global chemistry model, *J. Geophys. Res.*, *101*, 21,051-21,065, 1996.

Crutzen, P.J., Photochemical reaction initiated by and influencing ozone in unpolluted tropospheric air, *Tellus*, *26*, 45-55, 1974.

Crutzen, P.J., and M.O. Andreae, Biomass burning in the tropics: Impact on atmospheric chemistry and biogeochemical cycles, *Science*, *250*, 1669-1678, 1990.

Crutzen, P.J., and G.R. Carmichael, Modeling the influence of fires on atmospheric chemistry, in *Fire in the Environment: The Ecological, Atmospheric, and Climatic Importance of Vegetation Fires*, edited by P.J. Crutzen and J.G. Goldammer, pp. 89-106, John Wiley, New York, 1993.

Crutzen, P.J., and P.R. Zimmerman, The changing photochemistry of the troposphere, *Tellus*, *43A-B*, 136-151, 1991.

Crutzen, P.J., L.E. Heidt, J.P. Krasnec, W.H. Pollock, and W. Seiler, Biomass burning as a source of atmospheric gases CO, H_2, N_2O, NO, CH_3Cl, and COS, *Nature*, *282*, 253-256, 1979.

Crutzen, P.J., A.C. Delany, J. Greenberg, P. Haagenson, L. Heidt, R. Lueb, W. Pollock, W. Seiler, A. Wartburg, and P. Zimmerman, Tropospheric chemical composition measurements in Brazil during the dry season, *J. Atmos. Chem.*, *2*, 233-256, 1985.

Delmas, R., J.P. Lacaux, J.C. Menaut, L. Abbadie, X. Le Roux, G. Helas, and J. Lobert, Nitrogen compound emission from biomass burning in tropical African savanna FOS/DECAFE 1991 Experiment (Lamto, Ivory Coast), *J. Atmos. Chem.*, *22*, 175-193, 1995.

Dignon, J., and J.E. Penner, Biomass burning: A source of nitrogen oxides in the atmosphere, in *Global Biomass Burning: Atmospheric, Climatic, and Biospheric Implications*, edited by J.S. Levine, pp. 370 - 375, MIT Press, Cambridge, Mass., 1991.

Fishman, J., and V.G. Brackett, The climatological distribution of tropospheric ozone derived from satellite measurements using version 7 Total Ozone Mapping Spectrometer and Stratospheric Aerosol and Gas Experiment data sets, *J. Geophys. Res.*, *102*, 19,275-19,278, 1997.

Fishman, J., C.E. Watson, J.C. Larsen, and J.A. Logan, Distribution of tropospheric ozone determined from satellite data, *J. Geophys. Res.*, *95*, 3599-3617, 1990.

Fishman, J., J.M. Hoell Jr., R.D. Bendura, R.J. McNeal, and V.W.J.H. Kirchoff, NASA GTE TRACE-A experiment (September - October 1992): Overview, *J. Geophys. Res.*, *101*, 23,865-23,879, 1996.

Galloway, J.N., and G.E. Likens, Acid precipitation: The importance of nitric acid, *Atmos. Environ.*, *15*, 1081-1085, 1981.

Galloway, J.N., W.H. Schlesinger, H. Levy II, A. Michaels, and J.L. Schnoor, Nitrogen fixation: Anthropogenic enhancement - environmental response, *Global Biogeochem. Cycles*, *9*, 235-252, 1995.

Greenberg, J.P., P.R. Zimmerman, L. Heidt, and W. Pollock, Hydrocarbon and carbon monoxide emissions from biomass burning in Brazil, *J. Geophys. Res.*, *89*, 1350-1354, 1984.

Hao, W.M., and M.-H. Liu, Spatial and temporal distribution of tropical biomass burning, *Global Biogeochem. Cycles*, *8*, 495-504, 1994.

Hao, W.M., M.-H. Liu, and P.J. Crutzen, Estimates of annual and regional releases of CO_2 and other trace gases to the atmosphere from fires in the tropics, based on FAO statistics for the period 1975-1980, in *Fire in the Tropical Biota, Ecol. Stud. Ser.*, vol. 84, edited by J.G. Goldammer, pp. 440-462, Springer-Verlag, New York, 1990.

Herman, J.R., P.K. Bhartia, O. Torres, C. Hsu, C. Seftor, and E. Celarier, Global distributions of UV-absorbing aerosols from Nimbus 7/TOMS data, *J. Geophys. Res.*, *102*, 16,911-16,922, 1997.

Hsu, N.C., J.R. Herman, O. Torres, B.N. Holben, T.F. Eck, A. Smirnov, B. Chatenet, and F. Lavenu, Comparisons of TOMS aerosol index with the Sun-photometer aerosol optical thickness: Results and applications, *J. Geophys. Res.*, *104*, 6269-6279, 1999.

Hudson, R.D., and A.M. Thompson, Tropical tropospheric ozone from total ozone mapping spectrometer by a modified residual method, *J. Geophys. Res.*, *103*, 22,129-22,145, 1998.

Kasibhatla, P., H. Levy II, A.A. Klonecki, and W.L. Chameides, Three-dimensional view of the large-scale tropospheric ozone distribution over the North Atlantic Ocean during summer, *J. Geophys. Res.*, *101*, 29,305-29,316, 1996.

Kim, J.H., R.D. Hudson, and A.M. Thompson, A new method of deriving time-averaged tropospheric column ozone over the tropics using TOMS radiances: Intercomparison and analysis, *J. Geophys. Res.*, *101*, 24,317-24,330, 1996.

Kirchhoff, V.W.J.H., J.R. Alves, F.R. da Silva, and J. Fishman, Observations of ozone concentrations in the Brazilian cerrado during the TRACE A field expedition, *J. Geophys. Res.*, *101*, 24,029-24,042, 1996.

Klonecki, A.A., Model study of the tropospheric chemistry of ozone, Ph.D. thesis, Princeton Univ., Princeton, N. J.,1998.

Klonecki, A.A., and H. Levy II, Tropospheric chemical ozone tendencies in $CO\text{-}CH_4\text{-}NO_y\text{-}H_2O$ system: Their sensitivity to variations in environmental parameters and their application to a global chemical transport model study, *J. Geophys. Res.*, *102*, 21,221-21,237, 1997.

Levy, H., II, and W.J. Moxim, Simulated global distribution and deposition of reactive nitrogen emitted by fossil fuel combustion, *Tellus*, *41*, 256-271, 1989.

Levy, H., II, J.D. Mahlman, and W.J. Moxim, Tropospheric N_2O variability, *J. Geophys. Res.*, *87*, 3061-3080, 1982.

Levy, H., II, J.D. Mahlman, W.J. Moxim, and S.C. Liu, Tropospheric ozone: The role of transport, *J. Geophys. Res.*, *90*, 3753-3772, 1985.

Levy, H., II, W.J. Moxim, P.S. Kasibhatla, and J.A. Logan, The global impact of biomass burning on tropospheric reactive nitrogen, in *Global Biomass Burning: Atmospheric, Climatic, and Biospheric Implications*, edited by J.S. Levine, pp. 363-369, MIT Press, Cambridge, Mass., 1991.

Levy, H., II, P.S. Kasibhatla, W.J. Moxim, A.A. Klonecki, A.I. Hirsch, S.J. Oltmans, and W.L. Chameides, The global impact of human activity on tropospheric ozone, *Geophys. Res. Lett.*, *24*, 791-794, 1997.

Levy, H., II, W.J. Moxim, A.A. Klonecki, and P.S. Kasibhatla, Simulated tropospheric NO_x: Its evaluation, global distribution and individual source contributions, *J. Geophys. Res.*, *104*, 26,279-26,306, 1999.

Liu, S.C., M. Trainer, F.C. Fehsenfeld, D.D. Parish, E.J. Williams, D.W. Fahey, G. Hubler, and P.C. Murphy, Ozone production in the rural troposphere and the implications for regional and global ozone distributions, *J. Geophys. Res.*, *92*, 4191-4207, 1987.

Liu, H., W.L. Chang, S.J. Oltmans, L.Y. Chan, and J.M. Harisse, On springtime high ozone events in the lower troposphere from Southeast Asian biomass burning, *Atmos. Environ.*, *33*, 2403-2410, 1999.

Lobert, J.M., W.C. Keene, J.A. Logan, and R. Yevich, Global chlorine emissions from biomass burning: Reactive chlorine emissions inventory, *J. Geophys. Res.*, *104*, 8373-8389, 1999.

Logan, J.A., Nitrogen oxides in the troposphere: Global and regional budgets, *J. Geophys. Res.*, *88*, 10,785-10,807, 1983.

Mahlman, J.D., and W.J. Moxim, Tracer simulations using a global general circulation model: Results from a midlatitude instantaneous source experiment, *J. Atmos. Sci.*, *35*, 1340-1374, 1978.

Malingreau, J.-P., C.J. Tucker, and N. Laporte, AVHRR for monitoring global tropical deforestation, *Int. J. Remote Sens.*, *10*, 855-857, 1989.

Manabe, S., and J.L. Holloway Jr., The seasonal variation of the hydrologic cycle as simulated by a global model of the atmosphere, *J. Geophys. Res.*, *80*, 1617-1649, 1975.

Manabe, S., D.G. Hahn, and J.L. Holloway Jr.,The seasonal variation of the tropical circulation as simulated by a global model of the atmosphere, *J. Atmos. Sci.*, *31*, 43-83, 1974.

Marufu, L., J. Ludwig, M.O. Andreae, J. Lelieveld, and G. Helas, Spatial and temporal variation in domestic biofuel consumption rates and patterns in Zimbabwe: Implications for atmospheric trace gas emission, *Biomass Bioenergy*, *16*, 311-332, 1999.

Matthews, E., Global vegetation and land use: New high-resolution data bases for climate studies, *J. Clim. Appl. Meteorol.*, *22*, 474-487, 1983.

Matthews, E., Atlas of archived vegetation, land-use and seasonal albedo data sets, *NASA Tech. Mem.*, *86199*, 1985.

McKee, D.J. (Ed.), *Tropospheric Ozone, Human Health and Agricultural Impacts*, A.F. Lewis, New York, 1993.

Melinotte, J.M., O. Arino, and J.M. Rosaz, 1997: Multi year global fire atlas at 1 km, paper presented at EUMETSAT Users Conference, European Meteorological Satellite Organization (EUMETSAT), Bruxelles, Oct. 13-17, 1997.

Menaut, J.C., L. Abbadie, F. Levanu, P. Loudjani, and A. Podaire, Biomass burning in West African Savannas, in *Global Biomass Burning: Atmospheric, Climatic, and Biospheric Implications*, edited by J.S. Levine, pp. 133-142, MIT Press, Cambridge, Mass., 1991.

Moxim, W.J., Simulated transport of NO_y to Hawaii during August: A synoptic study, *J. Geophys. Res.*, *95*, 5717-5729, 1990.

Moxim, W.J., H. Levy II, and P.S. Kasibhatla, Simulated global tropospheric PAN: Its transport and impact on NO_x, *J. Geophys. Res.*, *101*, 12,621-12,638, 1996.

Nichol, J., Smoke haze in Southeast Asia: A predictable recurrence, *Atmos. Environ.*, *32*, 2715-2716, 1998.

Novelli, P.C., L.P. Steele, and P.P. Tans, Mixing ratios of carbon monoxide in the troposphere, *J. Geophys. Res.*, *97*, 20,731-20,750, 1992.

Olson, J.R., B.A. Baum, D.R. Cahoon, and J.H. Crawford, Frequency and distribution of forest, savanna, and crop fires over tropical regions during PEM-Tropics A, *J. Geophys. Res.*, *104*, 5865-5876, 1999.

Oort, A.H., Global atmospheric circulation statistics, 1958-1973, *NOAA Prof. Pap.*, *14*, 180 pp., Washington, D.C., 1983.

Prinn, R.G., R.F. Weiss, B.R. Miller, J. Huang, F.N. Alyea, D.M. Cunnold, P.J. Fraser, D.E. Hartley, and P.G. Simmonds, Atmospheric trends and lifetimes of CH_3CCl_3 and global OH concentrations, *Science*, *269*, 187-192, 1995.

Richardson, J.L., An investigation of large-scale tropical biomass burning and the impact of its emissions on atmospheric chemistry, Ph.D. thesis, Georgia Inst. of Technol., Atlanta, 1994.

Sachse, G.W., R.C. Hariss, J. Fishman, G.F. Hill, and D.R. Cahoon, Carbon monoxide over the Amazon Basin during the 1985 dry season, *J. Geophys. Res.*, *93*, 1422-1430, 1988.

Schultz, M.G., et al., On the origin of tropospheric ozone and NO_x over the tropical South Pacific, *J. Geophys. Res.*, *104*, 5829-5843, 1999.

Seiler, W., and P.J. Crutzen, Estimates of gross and net fluxes of carbon between the biosphere and the atmosphere from biomass burning, *Clim. Change*, *2*, 207-247, 1980.

Soares, R.V., Fire in some tropical and subtropical South American vegetation types: An overview, in *Fire in the Tropical Biota: Ecosystem Processes and Global Challenges*, edited by J. G. Goldammer, pp. 63-81, Springer-Verlag, New York, 1990.

Soden, B.J., and F.P. Bretherton, Interpretation of TOVS water vapor radiances in terms of layer-average relative humidities: Method and climatology for the upper, middle, and lower troposphere, *J. Geophys. Res.*, *101*, 9333-9343, 1996.

Spivakovsky, C.M., R. Yevich, J.A. Logan, S.C. Wofsy, M.B. McElroy, and M.J. Prather, Tropospheric OH in a three-dimensional chemical tracer model: An assessment based on observations of CH_3CCl_3, *J. Geophys. Res., 95,* 18,441-18,471, 1990.

Streets, D.G., and S.T. Waldhoff, Biofuel use in Asia and acidifying emissions, *Energy, 23*, 1029-1042, 1998.

Taylor, J.A., and P.R. Zimmerman, Modeling trace gas emissions from biomass burning, in *Global Biomass Burning: Atmospheric, Climatic, and Biospheric Implications*, edited by J.S. Levine, pp. 345-350, MIT Press, Cambridge, Mass., 1991.

Wesely, M.L., Parameterization of surface resistances to gaseous dry deposition in regional-scale numerical models, *Atmos. Environ.*, *23*, 1293-1304, 1989.

Wesely, M.L., and B.B. Hicks, Some factors that affect deposition [illegible] *Pollut. Control Assoc.*, *27*, 1110-1116, 1977.

World Meteorological Organization, WMO sectoral site survey on transboundary air pollution: Program to address ASEAN regional transboundary smoke (PARTS), report and recommendations, Geneva, 1997.

Yienger, J., A.A. Klonecki, H. Levy II, W.J. Moxim, and G.R. Carmichael, An evaluation of chemistry's role in the winter-spring ozone maximum found in the northern midlatitude free troposphere, *J. Geophys. Res.*, *104*, 3655-3667, 1999.

Ziemke, J.R., S. Chandra, and P.K. Bhartia, Two new methods for deriving tropospheric column ozone from TOMS measurements: Assimilated UARS MLS/HALOE and convective-cloud differential techniques, *J. Geophys. Res.*, *103*, 22,115-22,127, 1998.

G. R. Carmichael, Center for Global and Regional Environmental Research, University of Iowa, Iowa City, IA 52242. (gcarmich@icaen.uiowa.edu)

M. Galanter, Atmospheric and Oceanic Sciences Program, Princeton University, Princeton, NJ 08542. (mkg@gfdl.gov)

H. Levy II, Geophysical Fluid Dynamics Laboratory, P.O. Box 308, Princeton, NJ 08542. (hl@gfdl.gov)

(Received July 14, 1999; revised October 1, 1999; accepted November 4, 1999.)